FINAL REPORT

Colloidal Fouling of Reverse Osmosis Membranes

Contract D-92-01

Submitted to

National Water Research Institute
10500 Ellis Avenue
P.O.Box 20865
Fountain Valley, CA 92728-0865

December 28, 1994

by

MENACHEM ELIMELECH
ASSOCIATE PROFESSOR
DEPARTMENT OF CIVIL AND ENVIRONMENTAL ENGINEERING
UNIVERSITY OF CALIFORNIA
LOS ANGELES, CA 90024-1593

Table of Contents

EXECUTIVE SUMMARY

The general objective of this NWRI funded project was to better understand the role of chemical factors in colloidal fouling of reverse osmosis membranes. The results of this research are of paramount importance for efficient operation of RO installations used in water reclamation and reuse and in potable water treatment.

Fouling experiments of thin film composite and cellulose acetate reverse osmosis membranes by aluminum oxide and silica colloids were carried out. Membrane fouling was investigated at various solution chemistries under fixed hydrodynamic conditions (see Figure 1 for scope of work). Results show that the fouling rate increases with an increase in the ionic strength of the solution. Fouling was significant at high ionic strengths, including in the presence of background dissolved organic matter, resulting in a gradual decrease in product water flux and salt rejection. Under the chemical conditions tested, colloidal fouling was found to be reversible, thus indicating that pore blockage is not an important mechanism in colloidal fouling of reverse osmosis membranes.

A qualitative model for the role of chemical-colloidal interactions in colloidal fouling of reverse osmosis membranes is proposed. Fouling is controlled by particle–membrane and particle–retained particle interactions, which, in turn, are determined by solution chemistry, chemical properties of colloids and membranes, and the magnitude of permeation drag. At low ionic strengths, fouling is determined by an interplay between double layer repulsion and permeation drag.

The work described in this report resulted in several publications (see itemized list on page 4). Furthermore, we are in the progress of writing additional papers related to our recent colloidal fouling experiments and modeling.

One important conclusion of this work is that colloidal fouling cannot be eliminated by chemical means alone. For example, modifying the colloidal stability of suspended particles can reduce fouling but cannot prevent it. It is most likely that fouling can be minimized by physical (hydrodynamic) means. It is suggested to further investigate the role of hydrodynamics (more specifically, the control of permeation drag and cross flow velocity) in RO membrane fouling.

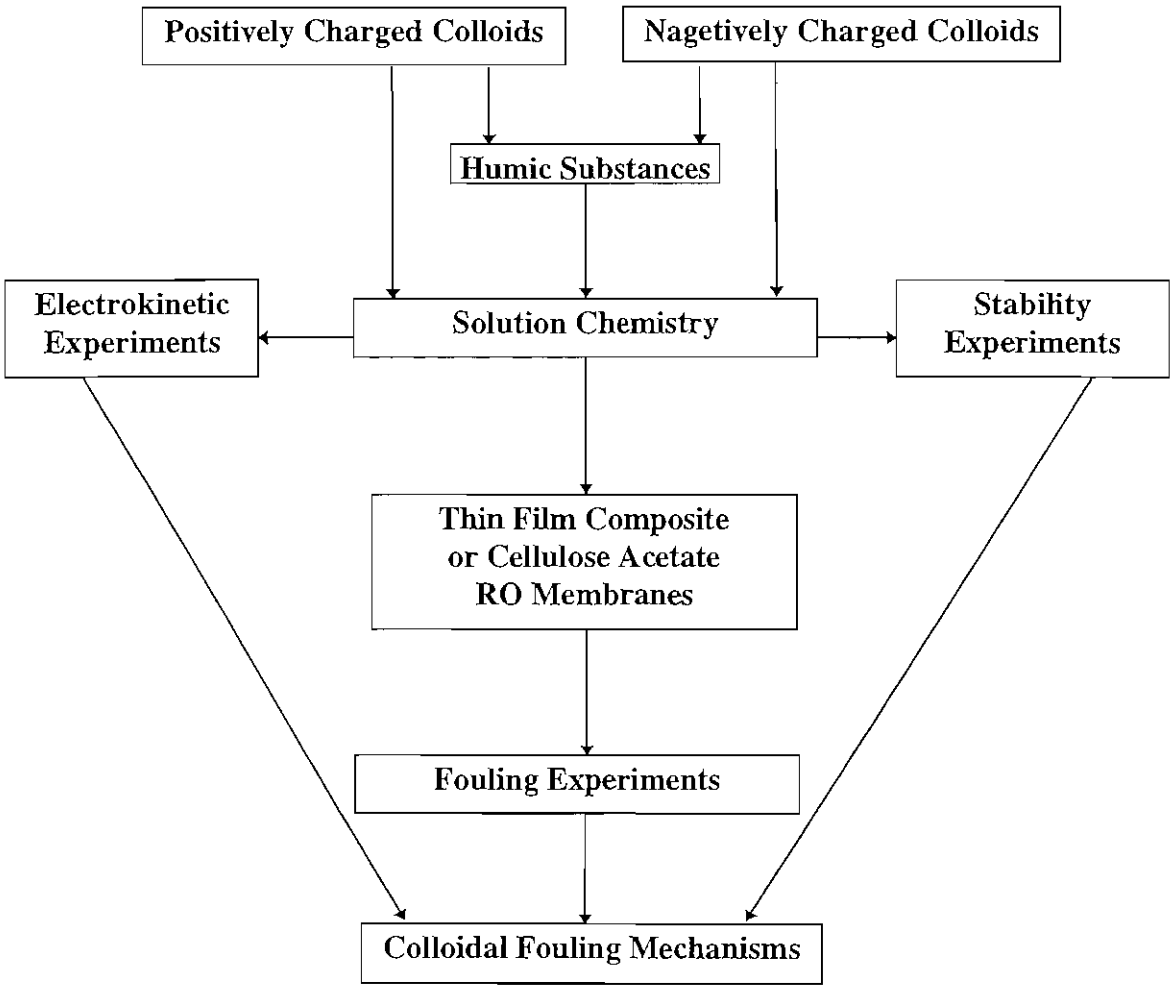

Figure 1: Schematic Description of Scope of Research

PUBLICATIONS ACKNOWLEDGING NWRI SUPPORT

Refereed Journal Publications

1. Elimelech, M., Chen, W. H., and Waypa, J. J. "Measuring the Zeta (Electrokinetic) Potential of Reverse Osmosis Membranes by a Streaming Potential Analyzer", *Desalination.*, Vol. 95(3), July 1994, pages 269-286 (see Appendix I).

2. Zhu, X., and Elimelech, M. "Fouling of Reverse Osmosis Membranes by Aluminum Oxide Colloids", submitted to: *Journal of Environmental Engineering, ASCE* (see Appendix II).

3. Song, L. and Elimelech, M. "Particle Deposition onto a Permeable Surface in laminar Flow", submitted to: *Journal of Colloid and Interface Science* (see Appendix III).

Conference Proceedings

1. Elimelech, M., and Zhu, X., "Colloidal Fouling of Reverse Osmosis Membranes", presented at the *Proceedings of the ASCE-1994 National Conference on Environmental Engineering*, July 11-13, 1994, pages 329-335 (see Appendix IV)

Note: The results of this work will be presented at, and published in proceedings of, the following professional meetings in 1995:

- 1995 AWWA Membrane Technology Conference (Reno, Nevada, August 13-16).
- 1995 North American Membrane Society Annual Meeting (Portland, Oregon, May 20-24).

Colloidal Fouling of TFCL RO Membranes by Colloidal Silica

The results presented in this section are of our recently completed work on the role of solution chemistry in fouling of TFCL-LP RO membranes by colloidal silica.

MATERIALS AND METHODS

Membranes

Low pressure thin film composite membranes were used in the fouling experiments with silica. These membranes, denoted as TFCL-LP, were supplied by Fluid Systems (San Diego, California). The TFCL-LP membrane is a highly cross-linked aromatic polyamide membrane and has a structure similar to the FilmTec FT-30. According to the manufacturer, the allowable operating pH range is from 4 to 11, the allowable feedwater temperature range is between 1 and 45°C, and the maximum operating pressure is 350 psi The manufacturer also claims that this membrane can tolerate 1,000 ppm-hr exposure to free chlorine. The nominal water flux is reported to be between 28 and 34 GFD and the minimum salt rejection 98.5% under test conditions of 2,000 ppm NaCl, 220 psi, 25°C, and pH of 7. This membrane was supplied as wet, flat sheet and was stored in 0.75% sodium metabisulfite solution at 4°C.

Colloidal Silica

Commercial silica particles (Aerosil 200) are used as model colloids in the fouling experiments (Degussa Corp., Akron, Ohio). The colloidal silica was supplied as a powder and has a BET surface area in the range of 175 to 225 m^2/g, an isoelectric point around 2, a density of 2.9 g/cm^3, and silanol group density of 2.6 $SiOH/nm^2$ (Degussa Technical

Bulletin 1990). The hydrodynamic diameter of the particles as measured by dynamic light scattering is 210 nm. The method for preparing the silica suspensions is similar to that used for aluminum oxide and has been described in Appendix II.

Reverse Osmosis Test Unit

The temperature control system in the fouling experiments with silica has been improved. An Isotemp Refrigerated Circulator Model 910 (Fisher Scientific, Pittsburgh, PA) with a stainless steel coil, is used to control the temperature. This new temperature control system allows us to eliminate the effects associated with seasonal temperature variations.

In all the RO fouling tests, the average fluid crossflow velocity over the membrane under the hydraulic conditions employed is 5.33 cm/s, resulting in a Reynolds number close to 450. In a typical test, the membranes are first equilibrated with deionized water for 17 hours, and then with a particle-free salt solution for additional 24 hours. After this period of equilibration (i.e. 41 hours) the flux is usually constant and all additional flux decline can be attributed solely to colloidal fouling. After equilibration, fouling experiment is initiated by adding a concentrated silica stock suspension to the feeding tank to establish the desired particle concentration.

All experiments were conducted at 250 psi effective transmembrane pressure and 20°C. Two pH values, 5.7 or 7.8, were used during the experiments.

REPRESENTATIVE RESULTS AND DISCUSSION

Electrokinetic Properties of Colloids and Membranes

The zeta potential of the colloidal silica as a function of solution pH and ionic strength is presented in Figure 2. As shown, the isoelectric point of the colloidal silica is approximately 3, which is consistent with previously reported studies. This means that the silica colloids were negatively charged during all our colloidal fouling tests (pH 5.7 or pH 7.8). It is seen that as the ionic strength decreases, the zeta potential becomes more negative. The influence of ionic strength on the zeta potential is attributed to the changes in the thickness of the diffuse double layer. At high ionic strengths, the diffuse double layer of colloidal silica compresses, resulting in a smaller electrokinetic (zeta) potential.

We have also conducted zeta potential measurements of thin film composite membranes (Childress, 1994). The results showed that the isoelectric point of this

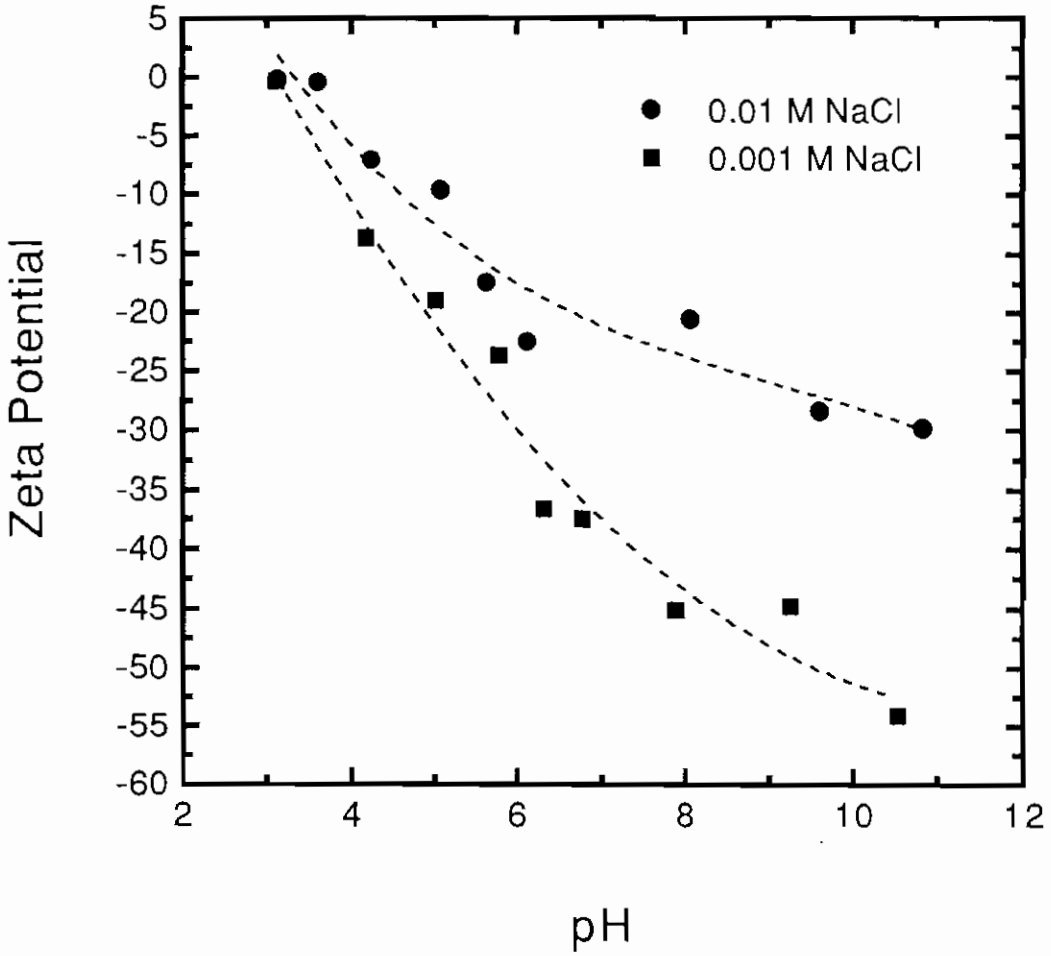

Fig. 2 Zeta potential of the colloidal silica as a function of pH for different ionic strengths

membrane is about 4.5. The membrane is therefore negatively charged at the pH values of our fouling experiments.

Colloidal Fouling Results

Representative fouling results are shown in Figures 3 to 9. The results are presented in terms of the relative water flux (or relative rejection) as a function of time. The relative flux (relative rejection) is the flux (rejection) at any time during the fouling test divided by the initial water flux (rejection) of the membrane, which is measured just before adding the particles at the end of the membrane equilibration time. The corresponding base line curves are also included in these figures. The base-line data are for the relative flux (relative rejection) in the test runs with a particle-free solution. The difference between the water flux (rejection) in the presence of particles and for the base line represents the net contribution of colloidal particles to membrane fouling.

Effect of Ionic Strength on Colloidal Fouling

Figure 3 illustrates the effect of ionic strength on the rate of colloidal fouling of the thin film composite membranes. These tests were carried out at three NaCl concentrations: 0.001 M, 0.01 M, and 0.1 M, respectively. Figure 3 shows that the rate and magnitude of membrane fouling by colloidal silica are more pronounced at higher ionic strengths. For instance, it is seen that after 50 hours since the addition of colloidal silica, the relative permeate flux drops increase from 25% to 35% when the ionic strength increases from 0.001 M to 0.1 M.

To explain the behavior observed in Figure 3 and subsequent figures, the interactions between the colloids and membranes have to be examined. As mentioned before, both colloidal silica and membrane surfaces are negatively charged at the solution pH investigated. Deposition of colloidal silica onto the membrane is, therefore, unfavorable. At lower ionic strengths, there exists a strong double layer repulsion between the newly approaching colloidal particles and the membrane surface or retained particles, whereas at higher ionic strengths, the double layer repulsion is significantly reduced. It is worthwhile to mention that in addition to the double layer repulsion, the permeation drag also plays an important role. This permeation drag is proportional to the permeation rate and has a direction pointing to the membrane surface (i.e., in opposite direction to the double layer repulsion). The permeation drag may overcome the double layer repulsion and cause significant deposition and fouling.

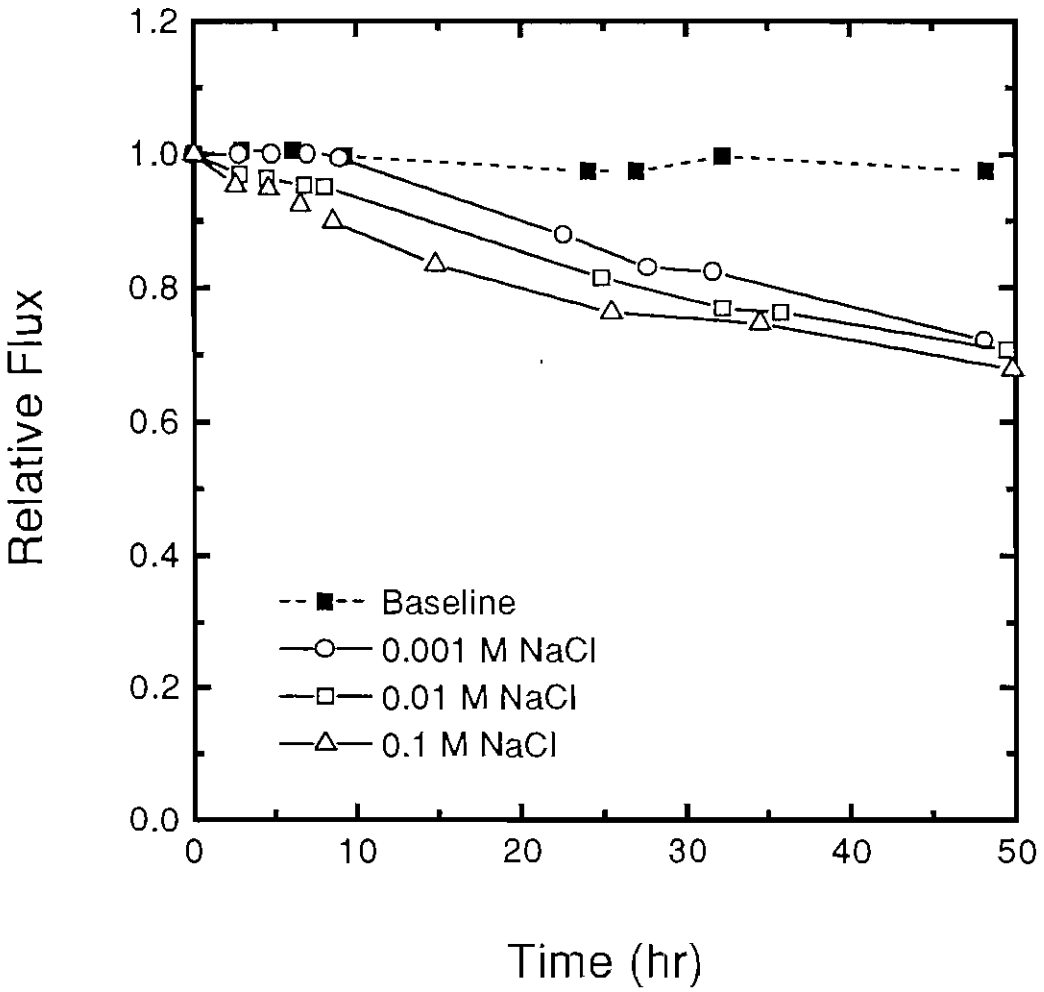

Fig. 3 Relative flux as a function of time for three different solution ionic strengths (30 mg/L SiO_2, pH 7.8)

The significant role of permeation drag is demonstrated by the run with 0.001 M NaCl where colloidal fouling is observed even in the presence of strong double layer repulsion. At high ionic strength (0.1 M), double layer repulsion is eliminated and colloids deposit onto the membrane surface by permeation drag, resulting in a thick foulant layer and a significant permeate water flux decline. The observed influence of ionic strength on colloidal silica is not pronounced compared to that with aluminum oxide, most likely due to differences in experimental conditions.

Effect of Permeation Drag

The effect of permeation drag is shown in Figure 4. In these experiments, permeation rate is controlled by varying the applied pressure. The results clearly demonstrate that higher permeation drag causes significant flux decline under given solution chemistry. When permeation drag triples from 125 psi to 375 psi, the permeate water flux decline increases four times, from 10% to 40%, after 50 hours of operation. The significant role of permeation drag is also demonstrated in Figure 3 by the run with 0.001M NaCl. At 0.001M ionic strength, silica particles are very stable and double layer repulsion is strong; therefore, the colloidal fouling observed is caused by permeation drag.

Effect of Particle Concentration

Figure 5 presents the effect of particle concentration on the rate of colloidal fouling at high ionic strength. Since the particle-particle interactions are more favorable at higher ionic strengths, the overall rate of colloidal deposition onto the membrane surface increases as the colloid concentration in the feedwater increases. Consequently, the thickness of the fouling layer increases resulting in reduced water fluxes.

The behavior of salt rejection in the presence of fouling is presented in Figure 6. This figure shows that the relative salt rejection decreases with time as the silica concentration increases. This may be attributed to two factors. The first results form the fouling layer that hinders back diffusion of salt from the membrane surface to the bulk feed and thus enhances concentration polarization. For higher silica concentrations, the hindrance is stronger since the foulant layer is thicker. The second reason is related to dilution effects. As the permeate water flux decreases, the salt concentration in the permeate increases and leads to a lower salt rejection.

Effect of pH on Colloidal Fouling

Figure 7 shows the effect of pH on colloidal fouling. There is no difference in flux decline between pH 5.7 and 7.8. Based on Figure 2, the zeta potential of silica colloids

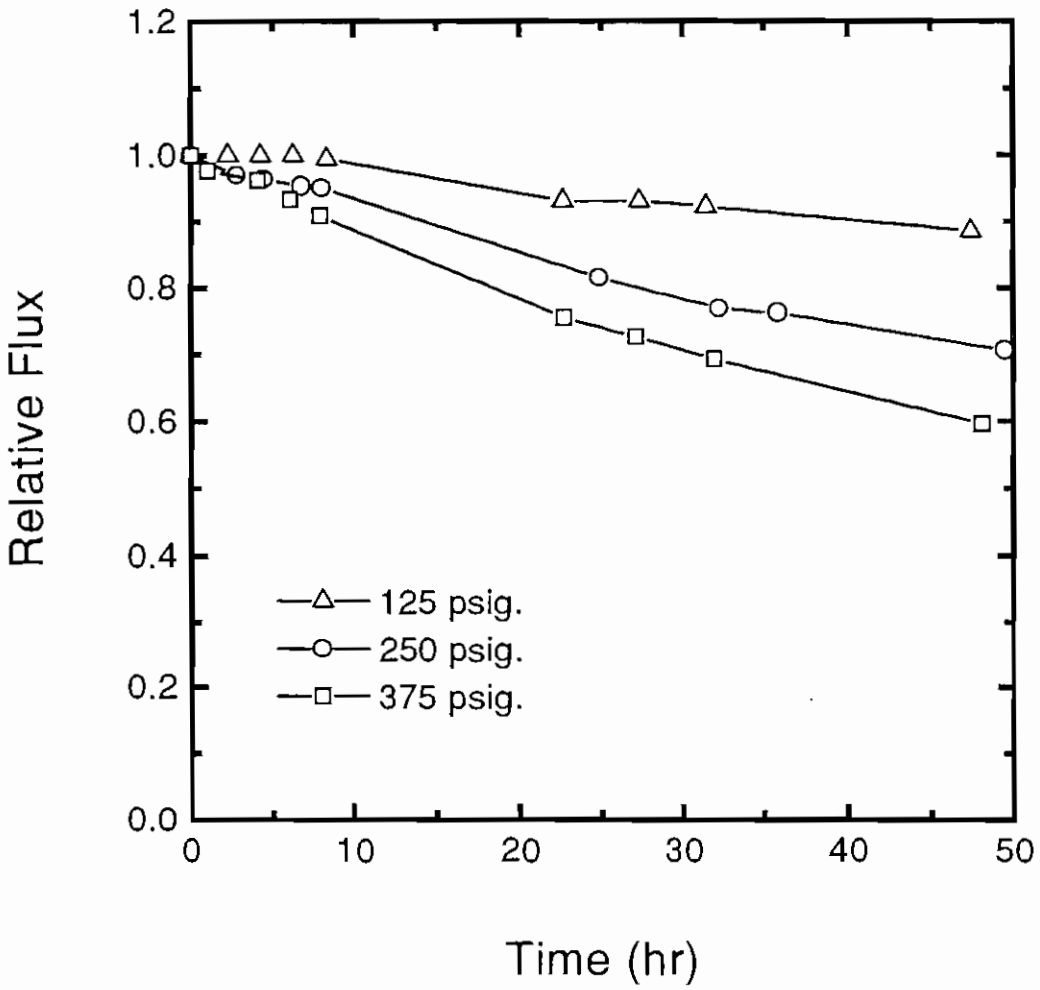

Fig. 4 Relative flux as a function of time for three different permeation pressures (0.01 M NaCl, 30 mg/L SiO_2, pH 7.8)

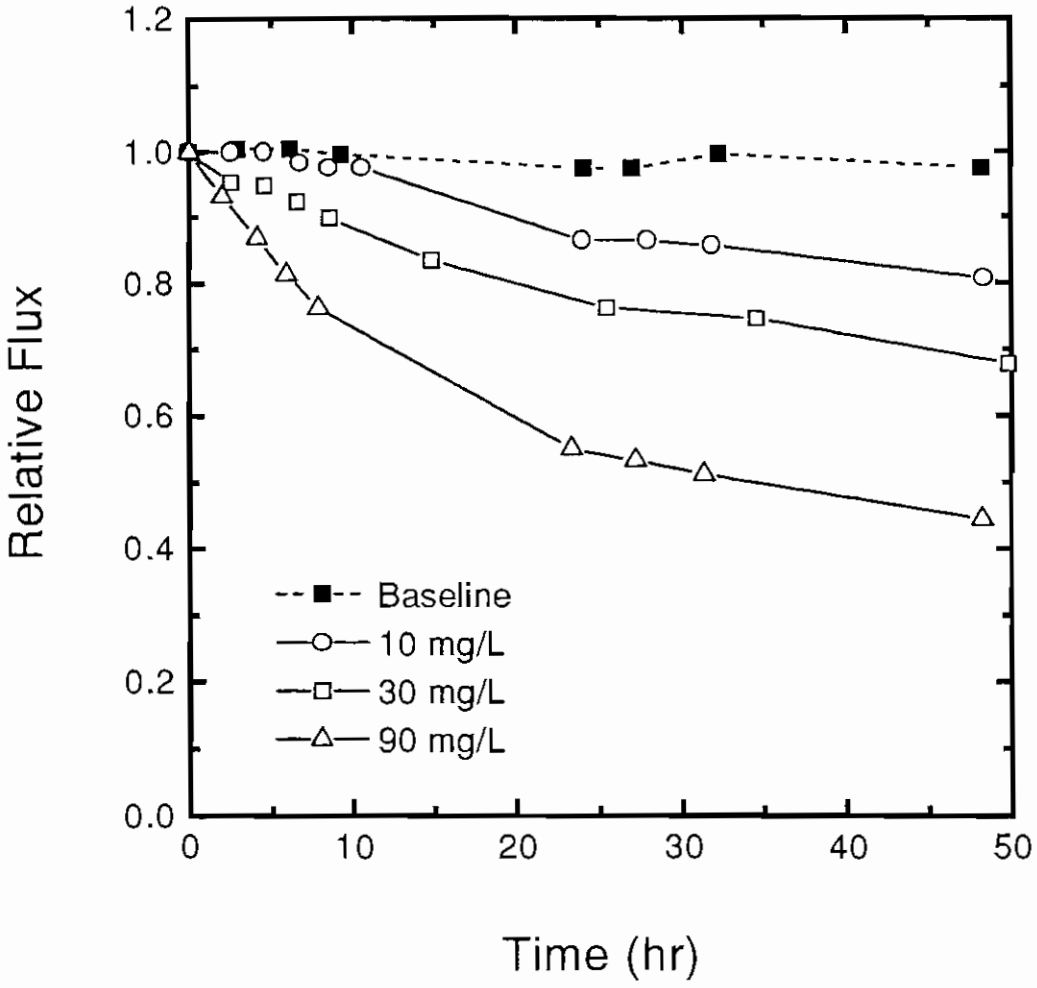

Fig. 5 Relative flux as a function of time for three different particle concentrations (0.1M NaCl, pH 7.8)

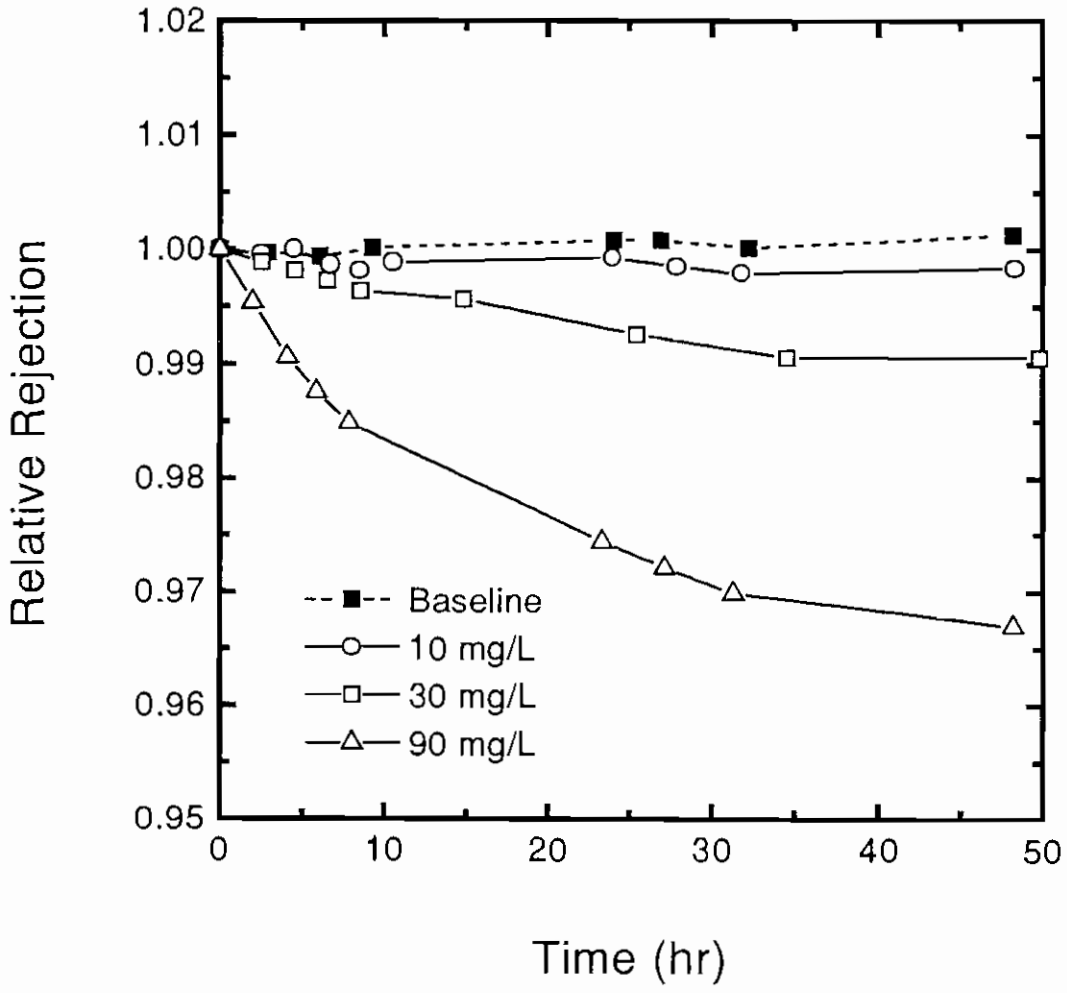

Fig. 6 Relative rejection as a function of time for three different particle concentrations (0.1 M NaCl, pH 7.8)

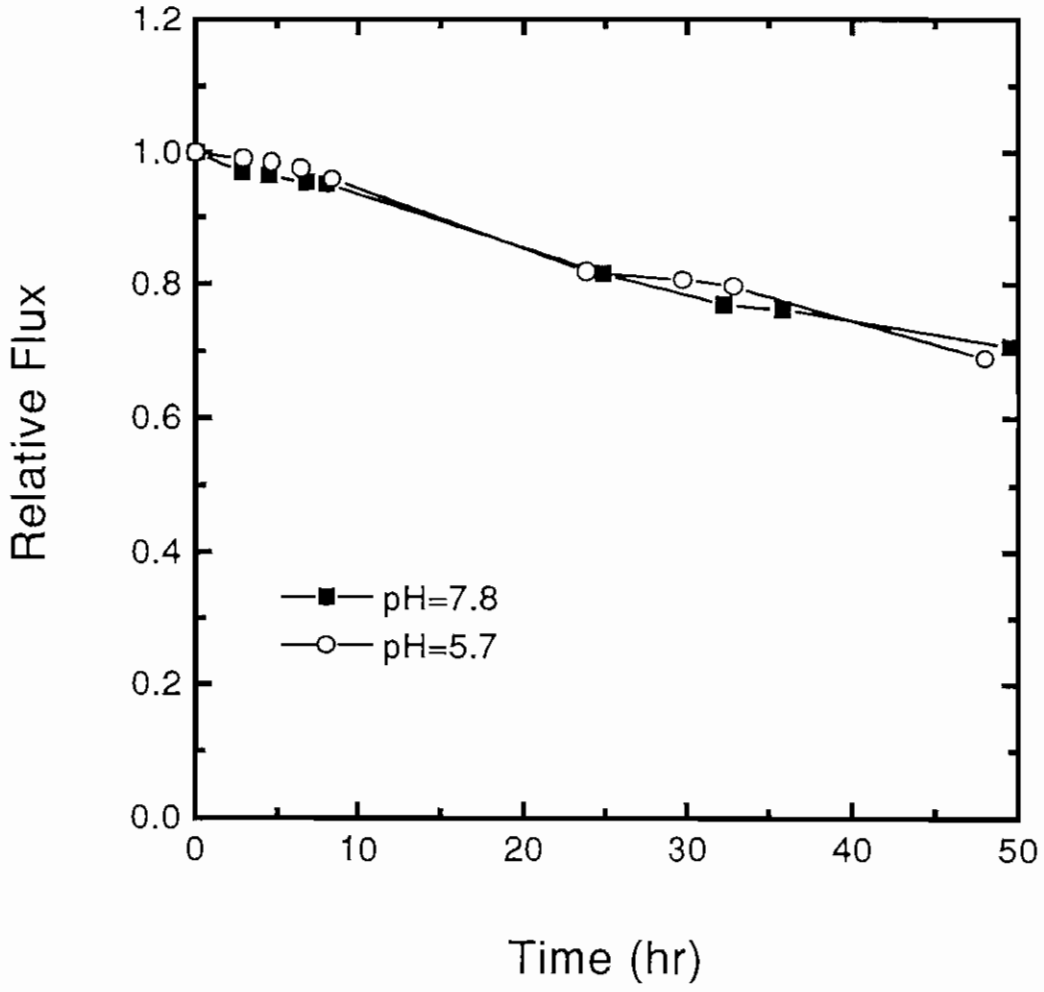

Fig. 7 Relative flux as a function of time for two different solution pH (0.01 M NaCl, 30 mg/L SiO_2)

becomes more negative at high pH (i.e. from -15 mV at pH 5.7 to -23 mV at pH 7.8), therefore, the double layer repulsion force should increase at higher pH. However, it is clearly shown that flux decline is not affected. This result indicates that under our testing conditions, permeation drag force dominates the double layer repulsion force. The same behavior is observed in testing the effect of divalent ions on fouling, as shown in Figure 8. Regardless of the electrolyte type and valence of ions, the flux decline curves are almost identical. The results shown in Figures 7 and 8 are interesting in that they are showing that particle deposition onto permeable surfaces may not be as sensitive to solution chemistry as the case with deposition onto impermeable solid surfaces.

Reversibility of Colloidal Fouling

Results of a typical reversibility experiment are shown in Figure 9. In this reversibility experiment, a fouling test similar to those described earlier was conducted for 50 hours. After 50 hours, the operation of the RO unit was stopped for a short period of time during which the membranes were gently removed from the cells and rinsed thoroughly with deionized water by a squeeze bottle. After rinsing the membranes and the cells, the membranes were placed back in the cells and operation was resumed for additional 50 hours of fouling. The experiments were performed at high silica concentration (90 mg/L colloidal silica) and high ionic strength (0.1 M NaCl) where fouling is expected to be significant.

Figure 9 shows that colloidal fouling by silica under the above chemical conditions is reversible and that the foulant can be removed by flushing with deionized water. The results indicate that colloidal fouling by silica is caused by increased resistance, and this additional resistance is due to accumulation of colloids on the membrane surfaces, not in the membrane pores as in the case of UF and MF membranes. Consistent with the results with aluminum oxide, it can be concluded that colloidal silica does not cause "pore blockage" during colloidal fouling.

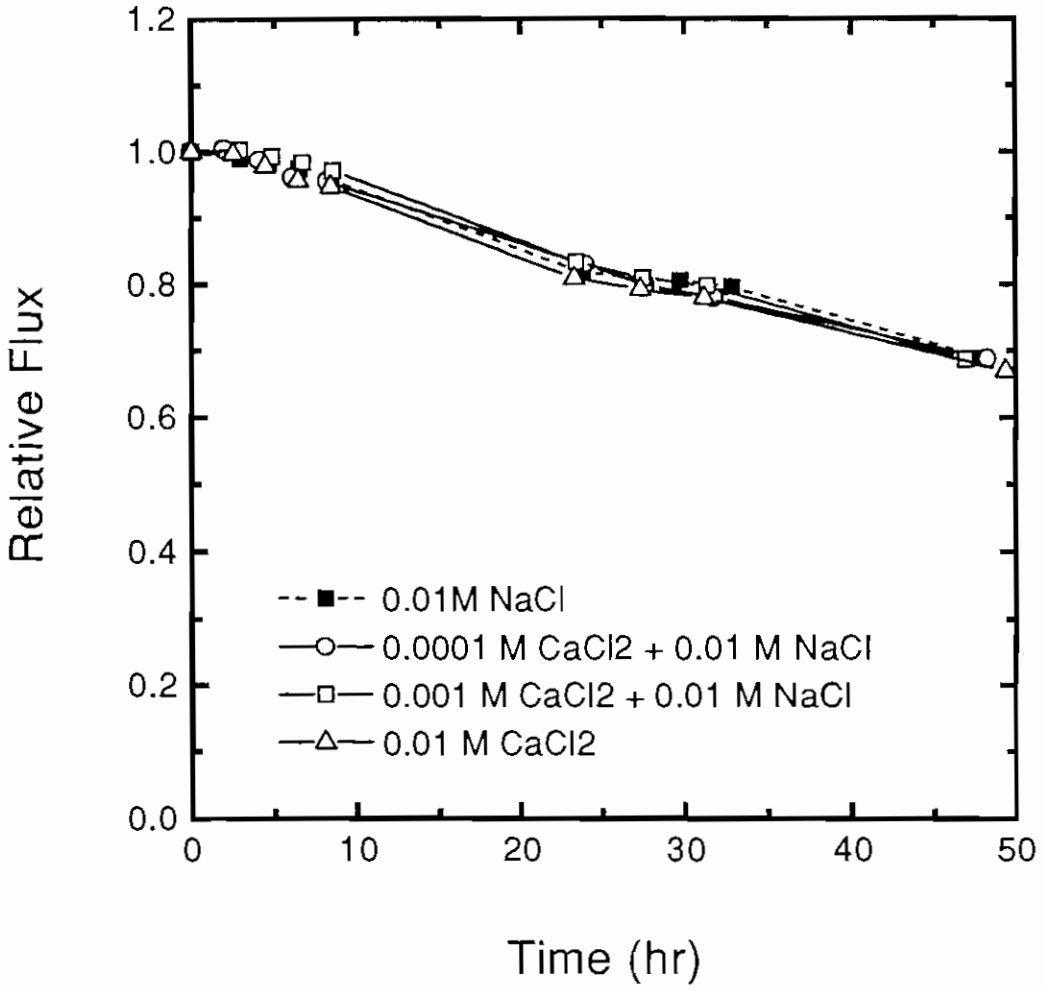

Fig. 8 Relative flux as a function of time for three different Ca^{2+} ion concentrations (30 mg/L SiO_2, pH 5.7)

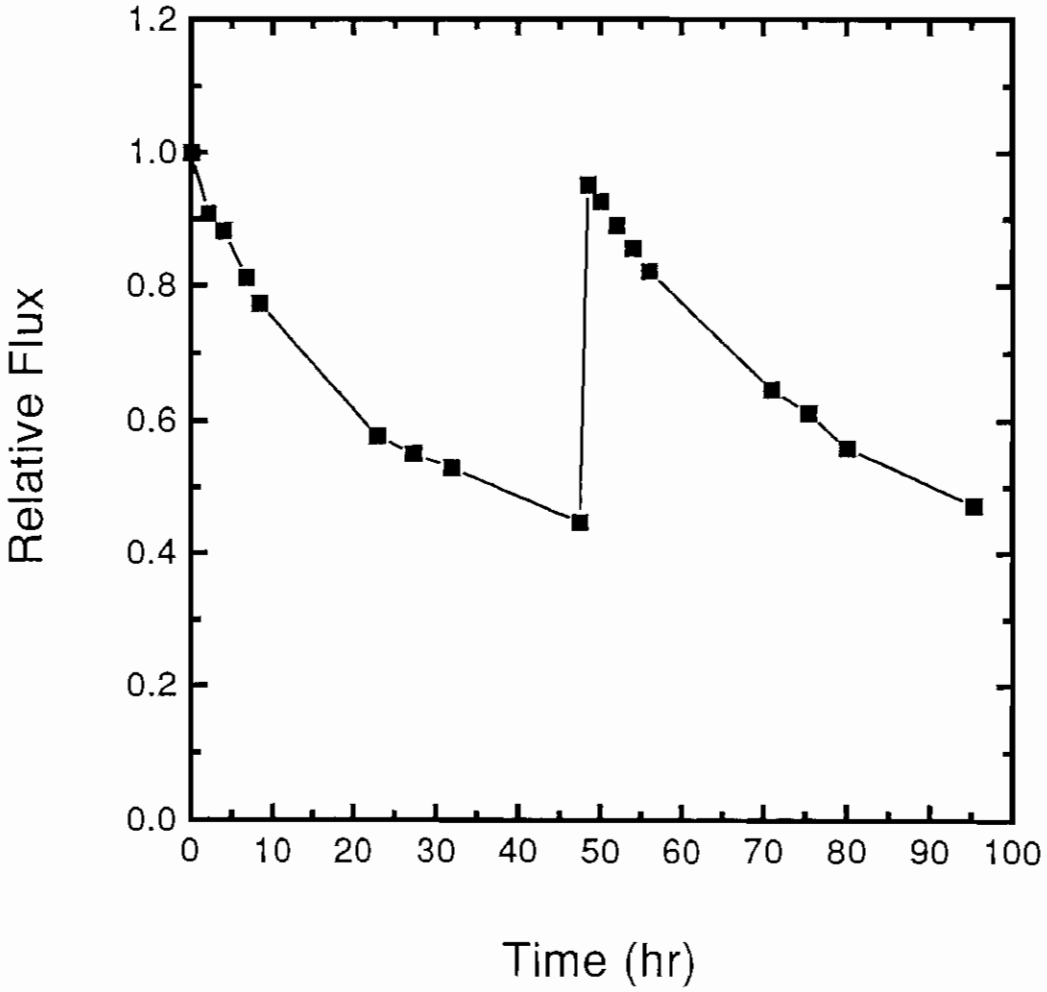

Fig. 9 Relative flux as a function of time before and after cleaning (0.1 M NaCl, 90 mg/L SiO_2, pH 5.7)

Appendix I

Elimelech, M., Chen, W. H., and Waypa, J. J. "Measuring the Zeta (Electrokinetic) Potential of Reverse Osmosis Membranes by a Streaming Potential Analyzer", ***Desalination***., Vol. 95(3), July 1994, pages 269-286.

Desalination, 95 (1994) 269–286
Elsevier Science B.V. Amsterdam — Printed in The Netherlands

Measuring the zeta (electrokinetic) potential of reverse osmosis membranes by a streaming potential analyzer

Menachem Elimelech,* William H. Chen and John J. Waypa

Department of Civil and Environmental Engineering, 4173 Engineering I, University of California, Los Angeles, CA 90024-1593 (USA)

(Received September 7, 1993; in revised form December 23, 1993)

SUMMARY

The use of a novel streaming potential analyzer to measure the zeta potential of cellulose acetate and composite polyamide reverse osmosis membranes is reported. Zeta potentials of these membranes were measured at various solution chemistries. These include effects of salt (NaCl) concentration, solution pH, and the presence of dissolved humic substances. It is demonstrated that streaming potential is a useful tool to measure zeta potential of reverse osmosis membrane surfaces. Results indicate that solution chemistry has a marked effect on the electrokinetic properties of reverse osmosis membranes. Humic substances strongly adsorb onto the surface of reverse osmosis membranes and thus alter the surface charge of the membranes. Furthermore, the zeta potential of reverse osmosis membranes becomes more negative as the NaCl concentration in solution increases, in a marked contrast to conventional electric double layer theories. It appears that the zeta potential of reverse osmosis membranes is strongly influenced by the presence of unreacted chemical substances or

*Author to whom correspondence should be addressed.

0011-9164/94/$07.00
SSDI 0011-9164(94)00064-U

The interaction of colloidal particles with membrane surfaces in aqueous media is dependent on, among other variables, the zeta (electrokinetic) potentials of the membrane surface and suspended particles. These, in turn, are controlled by the surface chemistry of the membranes and colloidal particles, as well as by the chemistry of the solution [5,8]. Hence, the determination of zeta potential of RO membranes at various solution chemistries is of paramount importance.

When brought into contact with an aqueous electrolyte solution, polymeric membrane surfaces acquire an electric surface charge through several mechanisms. These mechanisms include dissociation (ionization) of surface functional groups, adsorption of ions from solution, and adsorption of polyelectrolytes, ionic surfactants, and charged macromolecules [8]. The zeta potential is a measurable parameter, related to the charge and electric double layer of surfaces in aqueous solutions. For macroscopic surfaces, as in the case of polymeric RO membranes, the zeta potential can be determined by the streaming potential technique.

A limited number of studies have reported the use of streaming potential and electro-osmosis to characterize the electrokinetic potential of the interior pore surfaces in microporous membranes [9–12]. While the electrokinetic potentials of membrane pore surfaces can be important in colloidal fouling phenomena involving microfiltration or ultrafiltration membranes, these are probably not important in colloidal fouling of RO membranes. In RO membranes the pores (voids) are extremely small, on the order of a few angstroms [3]. It is most likely that, in colloidal fouling of RO membranes, colloids interact with the exterior surface of the membrane (i.e., the active layer), rather than with the interior pore surfaces.

Measurements of zeta potentials of RO membrane surfaces have not as yet been reported in the literature. The primary objective of this paper is to demonstrate the use of a novel streaming potential analyzer for measurement of zeta potential of RO membrane surfaces. The zeta potentials of cellulose acetate and composite polyamide membranes at various solution chemistries are reported. It is shown that solution chemistry plays an important role in controlling the zeta potential of polymeric RO membranes. Prior to presenting the experimental results, a discussion on the origin of surface charge of polymeric surfaces in aqueous solutions and a description of the basic principles and theory of the streaming potential method are presented.

hydrophobic polystyrene latex colloids [19–21]. It has been postulated that anions can approach more closely to nonpolar or hydrophobic surfaces because they are less hydrated than cations. In this process a surface will acquire a negative electrokinetic potential due to the presence of anions beyond the plane of shear. Jacobasch and Schurz [15] have developed expressions for determining the adsorption free energy of ions onto polymeric surfaces by means of zeta potential measurements. In addition, they unequivocally demonstrated that, in the presence of 1:1 simple electrolytes (such as NaCl), the zeta potential of various polymers becomes more negative as the contact angle of the polymer increases (i.e., as the polymer is more hydrophobic).

Adsorption of surfactants, polyelectrolytes, and charged macromolecules

Membrane surfaces can also acquire a surface charge through the adsorption of polyelectrolytes, ionic surfactants, and charged macromolecules [8,14,15]. The free energy of adsorption, ΔG_{ads}, of a solute is given by [8]

$$\Delta G_{ads} = \Delta G_{surf} - \Delta G_{solv} \tag{4}$$

where ΔG_{surf} represents the surface affinity for the solute and ΔG_{solv} is the solvent affinity for the solute. Thus, a solute that is hydrophobic in character will readily adsorb onto a solid surface. For polyelectrolytes adsorption arises from London-van der Waals interactions, hydrophobic bonding of nonpolar segments, hydrogen bonding, electrostatic attraction, and chemical reaction with surface functional groups. If the polyelectrolyte and the membrane surface are similarly charged, adsorption occurs if the non-electrostatic attraction is greater than the electrostatic repulsion. In this case adsorption is enhanced by increasing the ionic strength or by the presence of polyvalent counterions. If the polyelectrolyte and the surface are oppositely charged, then adsorption is dominated by electrostatic attraction.

THEORY AND PRINCIPLES OF STREAMING POTENTIAL

Electrokinetic effects

As described in the previous section, polymeric membranes acquire a

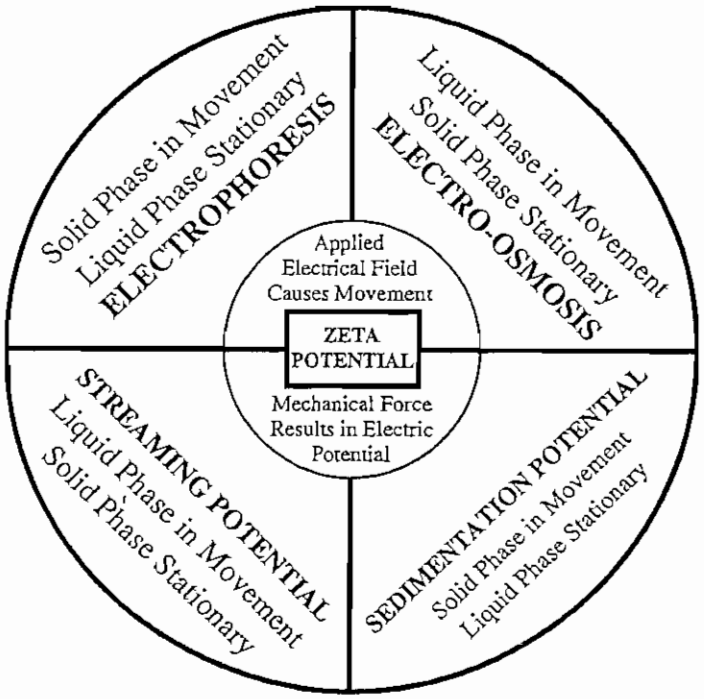

Fig. 1. Illustration of the four electrokinetic effects and their principles.

Streaming potential

When an electrolyte solution is forced, by means of hydraulic pressure, to flow through a porous plug of material, across a channel formed by two plates, or down a capillary, a streaming potential is generated. The liquid in the channel carries a net charge. Its flow, due to hydraulic pressure, gives rise to a streaming current, thereby generating a potential difference (Fig. 2). This potential opposes the mechanical transfer of charge, causing back conduction by ion diffusion and electro-osmotic flow (due to the potential difference). The transfer of charges due to these two processes is called the leak current (Fig. 2). When equilibrium condition is attained, the streaming current cancels the leak current, and the measured potential difference is the streaming potential [22,23].

The relationship between the measurable streaming potential and the zeta potential is given by the well known Helmholtz-Smoluchowski equation [14,15]:

$$\zeta = \frac{E_s}{\Delta P} \frac{\eta}{\varepsilon\varepsilon_0} \frac{L}{A} \frac{1}{R} \tag{5}$$

ing potential generated for a given, constant, driving pressure. For water at a given temperature, the values of η and ε are known. The electrical resistance across the channel, R, can be measured directly using an AC conductivity bridge. The L/A ratio can be determined as discussed above. Alternatively, using the Fairbrother and Mastin approach [15,25], this ratio can be replaced by $\kappa_s R_s$, where R_s is the electrical resistance of the channel when the measurement cell is filled with a standard solution whose specific conductance, κ_s, is known. A 0.1 M KCl solution is commonly used to avoid problems associated with surface conductance.

Finally, it should be mentioned that the Helmholtz-Smoluchowski theory was originally derived for a single capillary, and Eqn. (5) is an extension for bundles of capillaries or for a channel formed by two plates. Several assumptions were made in the derivation of Eqn. (5), most of which have been critically discussed by Christoforou et al. [26], Hunter [23], and Cohen and Radke [27]. While some of these assumptions are questionable for granular and porous materials, no apparent limitations exist in applying Eqn. (5) to a channel formed by two flat surfaces.

EXPERIMENTAL METHODS

Streaming potential analyzer

The measurements presented in this paper were carried out using a novel streaming potential analyzer (BI-EKA, Brookhaven Instruments Corp., Holtsville, New York, USA). The instrument includes an analyzer, a data control system, and measuring cells. The analyzer consists of a mechanical drive unit to produce and measure the pressure that drives the electrolyte solution from a reservoir into and through the measuring cell. Circulation of the solution is achieved by a pump with a flow capacity of 1.3 l/min. Operation can be controlled manually or by computer. The streaming potential as well as the streaming current are measured simultaneously by the instrument. Sensors for measuring the temperature, pH, and conductivity of the solution are also available.

There are two different measuring cells that can be used: cylindrical or rectangular. The choice of which cell to use depends on the nature of the sample under investigation. A cylindrical cell is used to measure the zeta potential of solid bodies such as fibers, granules, and rods. A rectangular

Membrane preparation

Membranes were rinsed thoroughly and soaked in deionized water for 24 h prior to the streaming potential measurements. Following this step, they were cut into 125×50 mm pieces to fit the rectangular cell. Two pieces of membranes were used for each measurement. One piece, with its active layer side facing down, was attached to the upper part of the cell; and the other piece, with its active layer side facing up, was attached to the lower part of the cell. The two pieces were separated by spacers that create a channel for the electrolyte solution to flow through. The cell was then tightened by screws on both ends and was attached to the streaming potential analyzer.

Determination of zeta potential

Before the start of each experiment, the cell was flushed with the electrolyte solution in both directions for a period of about 2 min to remove entrapped air bubbles from the cell. In a typical streaming potential measurement, the solution was pumped into the cell in alternating directions for a total of six times (three times in each direction). Each pumping period lasted 30 s. The reproducibility of the measurements was very good in both directions. The asymmetry potentials were below 0.5 mV, much smaller than the measured streaming potentials. The zeta potentials were calculated from the measured streaming potentials using Eqn. (5). The ratio L/A was determined using the Fairbrother and Mastin approach [15,25], as described earlier in this paper. The resistance of the channel, R, was calculated from the ratio of the streaming potential to the streaming current. Preliminary experiments demonstrated that, as expected, the generated streaming potential is linearly dependent on the applied pressure differential.

RESULTS AND DISCUSSION

Cellulose acetate membranes — Effect of solution pH and ionic strength

The effect of solution pH and ionic strength on the zeta potential of the cellulose acetate membranes is shown in Fig. 3. The zeta potential of the membranes was measured over the pH range of 3–11 for two different

and thus approach hydrophobic surfaces more favorably than hydrophilic ones.

The usual acetylating agent for cellulose is acetic anhydride. Excess compound is rinsed from the polymer with water and rapidly hydrolyzes to acetic acid. Traces of this weak acid are probably adsorbed on polymer particles and may influence the surface charge. The zeta potential curves shown in Fig. 3 are characteristic of surfaces with weak acidic functional groups.

It should be noted that in the production of cellulose acetate RO membranes, various chemicals (e.g., organic swelling agents) are added to improve the performance of the membranes. While these chemicals are not part of the cellulose polymer structure, they can still be attached to the membrane surface as impurities and, thus, influence the electrokinetic charge. Unfortunately, no information could be obtained from the manufacturer on the chemistry of these additives. It is possible that these impurities contain acidic functional groups, since the zeta potential of the membranes increases with pH, even at below neutral pH, much more than can be expected by adsorption of hydroxyl ions alone.

Composite membranes - Effect of solution pH and ionic strength

The effect of solution pH and ionic strength on the zeta potential of the composite polyamide membranes is shown in Fig. 4. As with the cellulose acetate, the zeta potential of the composite membranes was measured over the pH range of 3–11 for 0.001 and 0.01 M NaCl solutions. In addition, the zeta potential of the membrane was measured in deionized water over the above pH range. Based on the results shown in Fig. 4, the following observations are made: (1) the membrane is positively charged at low pH and negatively charged at pH values above the isoelectric point (pH 3.5); (2) the zeta potential curves at all ionic strengths intersect at the isoelectric point, indicating that there is no specific adsorption of cations; and (3) the zeta potential becomes more negative as the pH and ionic strength increase.

Before discussing the above observations, a brief description of the processes and chemicals involved in the synthesis of the composite polyamide membranes is offered. (More details can be found in [28].) This description provides a better understanding of the surface chemistry of the composite membrane and thus can explain the zeta potential data shown in Fig. 4.

ly charged at low pH (above about 2), while the apparent carboxyl groups are uncharged. As a result, the overall zeta potential of the composite polyamide membranes is positive at pH values smaller than 3.5. As the pH increases, acidic functional groups of carboxyl and remaining surfactants deprotonate, thus imparting a negative charge to the membrane. As with the cellulose acetate, the zeta potential of the composite membranes is more negative at higher salt concentrations, most probably due to adsorption of Cl^- from solution.

Effect of humic substances

Dissolved natural organic matter is ubiquitous in natural water bodies such as rivers, oceans, lakes, groundwaters, and estuaries [8,30,31]. The predominant fraction of dissolved natural organic matter in aquatic environments comprises humic substances. Humic substances are refractory anionic polyelectrolytes of low to moderate molecular weight. They contain both aromatic and aliphatic components with mainly carboxylic and phenolic functional groups [8,32]. Carboxylic functional groups account for 60–90% of all functional groups [33]. As a result, humic substances are negatively charged in the pH range of natural waters.

The configuration of humic substances is highly dependent on solution pH and ionic strength [8]. The characteristic lengths of humic substances are the hydrodynamic radius (when in solution) and the adsorbed layer thickness (when adsorbed on a surface). At high ionic strength or low pH, humic substances have a small hydrodynamic radius in solution and a large adsorbed layer thickness when adsorbed on the surface. On the other hand, at low ionic strength or high pH, humic substances have a large hydrodynamic radius and a small adsorbed layer thickness. Similar to polyelectrolytes, humic substances are readily adsorbed onto solid surfaces in aqueous solutions and markedly affect their electrokinetic charge [8,34,35]. Since RO is used for desalination of various natural waters, it is imperative that the effect of humic substances on the zeta potential of these membranes be investigated.

The effect of humic substances on the zeta potential of the cellulose acetate and composite polyamide membranes is illustrated in Figs. 5 and 6, respectively. In the study with the cellulose acetate membranes, humic substances with TOC levels of 0.7 and 1.4 mg/L were used, while for the composite membranes TOC levels of 0.3 and 0.7 mg/L were used. The

potential of RO membranes was reported. Effects of solution pH, ionic strength, and the presence of humic substances on the zeta potential of cellulose acetate and composite polyamide membranes were investigated. Based on the results reported in this paper, the following conclusions are made:

1. Streaming potential can be effectively used to measure the zeta potential of RO membranes.
2. Cellulose acetate and composite polyamide membranes are negatively charged at all pH values of practical interest (pH larger than 3.5).
3. The zeta potential of both membranes becomes more negative as the pH and the ionic strength of the solution increase.
4. Cellulose acetate and composite polyamide membranes acquire a negative surface charge through adsorption of anions from solution.
5. Humic substances adsorb onto membrane surfaces and markedly affect their zeta potential.
6. Chemical substances on membrane surfaces, which were introduced during the synthesis of the membranes, can markedly influence the electrokinetic charge and zeta potential of polymeric membranes.

Future research in this area should focus on measuring the zeta potential of **pure** cellulose acetate and aromatic polyamide polymers, rather than using commercial membranes whose surface properties are not completely known. Such research can result in a better understanding of the mechanisms involved in the development of surface charge of polymeric membranes in aqueous solutions. It is also suggested that the effect of various cleaning techniques on the zeta potential of RO membranes be investigated. Cleaning can remove adsorbed impurities from the membrane surface and thus alter the surface charge.

ACKNOWLEDGMENTS

The research reported in this paper was funded by the State of California, Department of Water Resources (DWR), and by the National Water Research Institute (NWRI). We would like to thank Brian Smith and Kurt Kovac from DWR and Ronald Linski from NWRI for their support and encouragement.

Appendix II

Zhu, X., and Elimelech, M. "Fouling of Reverse Osmosis Membranes by Aluminum Oxide Colloids", submitted to: ***Journal of Environmental Engineering, ASCE***.

Fouling of Reverse Osmosis Membranes by Aluminum Oxide Colloids

Submitted to

Journal of Environmental Engineering
American Society of Civil Engineers

October 1994

by

Xiaohua Zhu and Menachem Elimelech*
Department of Civil and Environmental Engineering
University of California
Los Angeles, CA 90024-1593

* To whom correspondence should be addressed.

water flux. Fouling of RO membranes places a large economic restriction on membrane plant operation. Hence, a fundamental understanding of the factors controlling the fouling of RO membranes is of paramount practical importance.

RO membrane foulants are usually classified into four major categories (Potts et al. 1981). These are (i) sparingly soluble salts, (ii) dissolved organic substances, (iii) colloidal and particulate matter, and (iv) biological growth. Among these foulants, colloidal particles are considered to be an important cause of membrane fouling (Brunelle 1980, Potts et al. 1981). Colloids are ubiquitous in all process waters and may include clays, iron oxide, colloidal silica, large organic macromolecules, organic colloids and suspended matter, and calcium carbonate precipitates (Stumm 1992).

Unlike the vast literature on fouling of ultrafiltration (UF) and microfiltration (MF) membranes, published research on the fouling of RO membranes is rather limited. One should bear in mind that fouling mechanisms of ultrafiltration and microfiltration membranes are not directly applicable to RO because of the great differences in membrane pore sizes and permeation rates. For instance, pore blockage is an important mechanism in the fouling of MF and UF membranes by colloids and macromolecules (Fane and Fell 1987, Wiesner et al. 1989, Lahoussine-Turcaud et al. 1990), but its role in RO membrane fouling is probably insignificant. Previous works on RO membrane fouling have focused primarily on precipitate fouling (e.g., Jackson and Landolt 1973, Gilron and Hasson 1987) and fouling by biological growth (e.g., Ridgway et al. 1984, 1985). However, the mechanisms of precipitate and biological fouling of RO membranes are quite different than those involved in colloidal fouling.

Only a few experimental studies on colloidal or particulate fouling of RO membranes are available in the literature. Winfield (1979a, 1979b) has investigated the fouling of cellulose acetate RO membranes by secondary wastewater effluents and has concluded that dissolved organic materials play a much more significant role in membrane fouling than large suspended particles. The findings of Winfield, however, are not conclusive due to the great variability in the chemical properties of colloids and dissolved organic materials in secondary wastewater effluents. In a later study by Cohen and Probstein (1986), the fouling rate of cellulose acetate RO membranes by colloidal ferric hydroxide was reported. Fouling was related to the foulant layer growth and a linear dependence between permeate flux and foulant layer thickness was found for the initial stages of fouling. The solution chemistry in their study, however, was limited to deionized water so that the role of chemical-colloidal interactions in membrane fouling could not be investigated.

At this writing, the mechanisms of colloidal fouling of RO membranes are poorly understood. The general objective of the present paper is to better understand the role of chemical-colloidal interactions in colloidal fouling of RO membranes. More specifically, in

Solution Chemistries

The NaCl and $CaCl_2$ salts used were analytical reagent grade (Fisher Scientific, Pittsburgh, Pennsylvania). All solutions and suspensions were prepared with deionized water of conductivity less than 1 μmhos/cm (Nano Pure II, Barnstead, Dubuque, Iowa). When necessary, pH adjustments were done by adding small amounts of HCl or NaOH. Commercial humic acid (Aldrich Chemical Company, Milwaukee, Wisconsin) was used in some of the fouling experiments. The humic acid stock solution was prepared by dissolving a known amount of the granular humic material in deionized water and adjusting the pH to about 11. The solution was agitated for 24 hours, and the pH was adjusted to 8 after this mixing time. Following this step, the solution was filtered through coarse glass filter and then through a 0.2 μm Millipore filter. The filtration rate through the 0.2 μm filter was extremely slow because of surface clogging, and filters were replaced frequently to allow a reasonable amount of dissolved humic materials to be collected. The TOC of the resulting stock solution was 1355 mg/L. The stock solution was stored in a refrigerator at 4°C.

Electrokinetic Properties of Colloids and Membranes

Electrophoretic mobility of the aluminum oxide colloids under various chemical conditions was measured by microelectrophoresis (Lazer Zee Model 501, Pen Kem Inc., Bedford Hills, New York). The instrument is equipped with a laser beam for illumination of the particles, a TV monitor for viewing the particles, and a rotating prism. With the rotating prism, the average mobility of many particles is determined simultaneously at each measurement. This technique is imperative for measuring the electrophoretic mobility of very small particles as those used in this research.

Zeta potentials of the RO membranes were determined by a novel streaming potential analyzer (BI-EKA, Brookhaven Instruments Corp., Holtsville, New York). The streaming potential as well as the streaming current are measured simultaneously by the instrument. The zeta potential for each solution chemistry was calculated from the corresponding measured streaming potential using the Helmholtz-Smoluchowski equation (Hunter 1981). A detailed description of the instrument and these measurements is given elsewhere (Elimelech et al. 1994).

Colloid Stability

The colloidal stability of the aluminum oxide particles was determined by coagulation experiments in 20 mL glass vials. A suspension of 100 mg/L particles was filled into the vials, and the solution chemistry of each vial was adjusted by adding the appropriate

was determined from the measured feed and permeate conductivities (YSI 32, Yellow Springs Instrument Co., Yellow Springs, Ohio). In addition, samples from the feeding tank were taken once or twice a day to measure the turbidity and the particle size of the suspension by dynamic light scattering.

In all experiments, the transmembrane pressure (*i.e.*, the applied pressure minus the bulk osmotic pressure) was maintained at 400 psi, so that the role of solution chemistry on the extent of colloidal fouling can be investigated without considering pressure effects. The pH of the feed suspension during the fouling experiments ranged from 5.6 to 6.0 and the average temperature was about 22°C. Under the above operating conditions, the average water flux after 14 hours of equilibration was about 1.2×10^{-5} and 0.7×10^{-5} m/s, for the thin film composite and the cellulose acetate membranes, respectively.

RESULTS AND DISCUSSION

Electrokinetic Properties of Colloids and Membranes

The electrophoretic mobility of the aluminum oxide colloids as a function of solution pH and concentration of dissolved humic substances (expressed as mg/L TOC) is presented in Fig. 2. As shown, the isoelectric point of the aluminum oxide colloids in the absence of humic substances is approximately 8.5, which is consistent with previous studies using these colloids (Kummert and Stumm 1980, Stone 1990, Stumm 1992). As the concentration of humic substances increases, the isoelectric point shifts to a lower pH. With 0.6 mg/L TOC in solution, the isoelectric point is about 3.5; the particles are negatively charged at pH values above this point.

The marked influence of humic substances on the electrophoretic mobility of the colloids indicates that humic substances strongly adsorb onto the surface of the aluminum oxide colloids. Humic substances are comprised of macromolecules with ionogenic functional groups; carboxyl is among the most abundant oxygen-containing functional groups (Liang and Morgan 1990, Morel and Hering 1993). These anionic macromolecules may adsorb onto the aluminum oxide colloids through one or more of the following mechanisms (Stumm 1992): (i) electrostatic attraction between negatively charged functional groups of the humic macromolecules and positively charged sites of the aluminum oxide, (ii) specific chemical interaction between humic carboxyl functional groups and OH-groups on the aluminum oxide, and (iii) hydrophobic interactions between the particles and non-polar segments of the humic macromolecules. Regardless of the mechanism of adsorption, the electrokinetic charge of the particles becomes more negative due to the negatively charged functional groups of the humic macromolecules adjacent to the Stern layer.

macromolecules adsorb onto the colloids in a flat configuration (Yokoyama et al. 1989, O'Melia and Tiller 1993). Tiller and O'Melia (1993) have shown that, under similar conditions, steric stabilization of humic-coated hematite colloids is not possible, even at high ionic strength where the range of double layer forces is very small. They attributed their results to the flat conformation of the humic macromolecules which do not extend sufficiently into the solution to cause steric stabilization. Hence, the observed coagulation behavior of the aluminum oxide in the presence of humic substances can be explained qualitatively by classical double layer theories. The humic-coated particles are stable at low ionic strengths because of the long range and large magnitude of interparticle double layer repulsion, while they are unstable at high ionic strength due to compression of their electric double layers.

The colloidal stability of the aluminum oxide colloids under various solution chemistries is very important for understanding the fouling behavior of the RO membranes. When colloids are unstable, they deposit onto previously retained particles resulting in a thick fouling layer. Detailed discussion of this important aspect is given later in the paper.

Effect of Ionic Strength on Colloidal Fouling

Accelerated fouling tests, demonstrating the effect of ionic strength on membrane fouling, are presented in this section. Accelerated fouling tests were carried out at high particle concentrations (100 mg/L) so that fouling may be observed within reasonable time scales (i.e., within 100 hours of operation). Other experiments, presented in subsequent sections, were carried out at lower particle concentrations (10 mg/L), which may be more typical of actual fouling conditions.

Representative fouling results with thin film composite membranes are shown in Fig. 4. These tests were conducted at three NaCl concentrations: 0.001, 0.01, and 0.1 M (58.4, 584.5, 5845.0 ppm, respectively). The results are presented in terms of the relative water flux as a function of time. The relative flux is the flux at any time during the fouling test divided by the initial water flux through the membrane, just before adding the particles at the end of the membrane equilibration time. The corresponding base line curves for each ionic strength are also included in this figure. The base-line data are for the relative flux in test runs with a particle-free solution. The difference between the water flux with particles and the base line represents the net contribution of colloidal particles to membrane fouling.

The base line curves show that water flux decline is obtained even in the absence of colloidal particles in solution. The decrease in permeate water flux in the base line experiments may be attributed to membrane compaction, concentration polarization effects,

of the thin film composite, the permeation drag in this case may be smaller than the double layer repulsion force and, as a result, particles cannot deposit onto previously retained particles. On the other hand, at 0.1 M NaCl, double layer repulsive forces are significantly reduced and particles deposit favorably onto previously retained particles, forming a thick fouling layer. This thick fouling layer significantly increases the resistance to water flow, thus reducing the water flux through the membrane.

Figure 6 illustrates the effect of particle concentration on the rate of colloidal fouling of thin film composite membranes at high ionic strength. As expected, under favorable particle–particle interactions, the overall rate of particle deposition onto the membrane increases as the bulk particle concentration increases. Consequently, the thickness of the fouling layer increases and the permeation water flux decreases at a higher rate.

The results shown in Figs. 4 and 5 suggest that an interplay between double layer repulsion and permeation drag may be important in colloidal fouling of RO membranes. It was also shown that particle–membrane and particle–retained particle interactions are key factors controlling the extent of colloidal fouling. These important aspects and additional discussion on the mechanisms of colloidal fouling are given in more details later in this paper.

An interesting observation in the fouling experiments discussed above (and those described later in this paper) is that membrane salt rejection decreases over time in the presence of colloidal fouling. This phenomenon was much more pronounced with the cellulose acetate membranes compared to the thin film composite membranes. The decrease in salt rejection (or increase in salt passage) may be attributed to several factors. The first is related to the poor mixing within the fouling layer which enhances concentration polarization and thus increases the passage of salt through the membrane. Such an effect was also observed in cellulose acetate membranes which were subject to biological fouling (Ridgway 1984, 1985). The second reason may be attributed to the reduced permeate water fluxes as fouling occurs, the so-called "dilution effect". As the permeate water flux decreases, the salt concentration in the permeate increases thus resulting in lower salt rejection. We are currently investigating systematically the effect of colloidal fouling on salt passage through RO membranes and will present the results in future publications.

Effect of Humic Substances

Humic substances are the predominant fraction of dissolved natural organic matter (Stumm 1992, Morel and Hering 1993). The effect of humic substances on colloidal fouling should be investigated because most feed waters for RO contain measurable levels of

experimental results. This aggregation problem is inherent of closed-loop laboratory RO units operating at chemical conditions where particles in suspension are unstable. Samples taken from the feed suspension showed that the particle size measured immediately after sampling increased much less than that under similar chemical conditions in the static coagulation experiments. This is most likely because of aggregate breakage induced by the mixing in the feeding tank and because of the hydrodynamic shear created as the suspension flows through the narrow stainless still tubes and the various accessories of the closed-loop RO system. The use of a flow-through RO unit (instead of a closed-loop unit) in such controlled fouling experiments is prohibitive because of the excessive quantities of deionized water and chemicals needed for each fouling test.

Reversibility of Colloidal Fouling

To better understand the mechanisms of colloidal fouling, experiments were conducted to test the reversibility of colloidal fouling. In reversibility experiments, a fouling test similar to those described earlier was conducted for 100 hours. After 100 hours, the operation of the RO unit was stopped for a short period of time during which the membranes were gently removed from the cells and rinsed thoroughly by deionized water with a squeeze bottle. After rinsing the membranes and the cells, the membranes were placed back in the cells and operation was resumed for additional 100 hours of fouling.

Results of typical reversibility experiments for a thin film composite membrane and a cellulose acetate membrane are shown in Figs. 8(a) and 8(b), respectively. These experiments were conducted with 10 mg/L aluminum oxide colloids and high ionic strength (0.1 M NaCl) where fouling is significant. The results for both membranes show that flushing with deionized water is sufficient to remove the fouling layer and restore the water flux to a level comparable to that with no particles in solution. The flux of the thin film composite membrane is not restored to its initial value, but the corresponding base line data show that the flux after cleaning is about what expected for operation with a particle-free 0.1 M NaCl solution for a period of 100 hours. The water flux of the cellulose acetate membrane, on the other hand, is completely restored after cleaning with deionized water. After cleaning, the fouling behavior is similar to that observed in the first 100 hours of operation as evident from the shape of the relative flux curves.

The data shown in Fig. 8 indicate that fouling by aluminum oxide colloids under the above chemical conditions is reversible. The results also strongly suggest that aluminum oxide particles do not bind to the membrane surface or block pores in the membrane (the so-called "pore blockage") as usually the case with UF and MF membranes. Fouling is caused

and deposition of the submicron aluminum oxide colloids used in this research. The transport mechanisms which mostly apply to our system are the permeation drag force which acts perpendicular to the membrane surface and double layer repulsion which acts in opposite direction to the permeation drag. The theoretical investigation of Song and Elimelech (1994) has shown that at very small permeation drags (i.e., for small permeation fluxes), double layer repulsion may significantly hinder the rate of particle deposition onto the membrane surface. However, as the permeation flux through the membrane increases, permeation drag may overcome double layer repulsion and thus result in particle deposition even at strong double layer repulsions between the particles and membrane. When the permeation drag is large enough, as in the case of UF membranes, permeation drag completely dominate the rate of particle deposition and double layer repulsion does not play any role in particle deposition. It is most interesting to note that the transition from double layer repulsion dominated deposition regime to permeation drag controlled deposition regime occurs at permeation velocities that fall in the range of those employed in RO membranes. Cellulose acetate membranes usually display smaller permeation fluxes than thin film composite membranes (at a comparable applied pressure). Therefore, we should expect that the interplay between double layer repulsion and permeation drag will have a direct effect on colloidal fouling of RO membranes as discussed below.

Colloidal Fouling Mechanisms

Based on the results presented in the present paper, analysis of transport and deposition mechanisms in cross flow membrane filtration (e.g., Chellam and Wiesner 1992, Song and Elimelech, 1994), and the vast literature on particle deposition onto non-permeable surfaces (e.g., Elimelech 1994ab, Song and Elimelech 1993), we propose the following qualitative mechanistic model for colloidal fouling of RO membranes. The fouling behavior of RO membranes in our model is related to solution chemistry, stability of the colloids, electrokinetic charge of particles and membranes, and permeation drag. Four different fouling scenarios, based on the ionic strength and electrokinetic charge of colloids and membranes, are discussed. These cases are for (1) moderate to high ionic strength, particles and membranes are oppositely charged; (2) moderate to high ionic strength, particles and membranes are similarly charged; (3) low ionic strength, particles and membranes are oppositely charged; and (4) low ionic strength, particles and membranes are similarly charged.

(1) Moderate to high ionic strength, particles and membranes are oppositely charged. In this case, the initial deposition of particles onto the oppositely charged membrane surface

Because of the low ionic strength, a strong lateral double layer repulsion exists between retained particles, and the initial density of surface coverage is not too high (Adamczyk et al. 1994). Under these conditions, there also exists a strong double layer repulsion between retained particles and approaching suspended particles. It is postulated that in this case the extent of colloidal fouling will depend on the interplay between double layer repulsion and permeation drag. For RO membranes operating at high permeation rates, permeation drag may overcome double layer repulsion between approaching and retained particles, resulting in the formation of a fouling layer on the membrane surface. Consequently, the permeation flux and salt rejection will be reduced as discussed before. On the other hand, when operating at small permeation rates, double layer repulsion may overcome the opposing permeation drag and fouling will be minimized.

(4) Low ionic strength, particles and membranes are similarly charged. In this case, a strong double layer repulsion exists between particles and membrane surface. The extent of particle deposition, and subsequently membrane fouling, is dependent on the interplay between double layer repulsion and permeation drag. When operating at small permeation rates, particle deposition may be prevented by the strong double layer repulsion and no fouling will occur. On the other hand, at high permeation rates, as encountered in most operations of thin film composite RO and nanofiltration (NF) membranes, particles may deposit onto the membrane surface and onto previously retained particles because of the strong permeation drag. In this case, fouling can be significant for waters containing measurable levels of suspended colloidal particles.

CONCLUSIONS

Based on the results reported in the present paper, the following conclusions are drawn:

1. Colloidal fouling of RO membranes results in reduced permeate water flux and salt rejection. The decrease in permeation rate is attributed to the greater resistance to water flow as colloids deposit onto the membrane and form a fouling layer. Increased salt passage (or reduced salt rejection) may be attributed to the poor mixing within the fouling layer which results in enhanced concentration polarization at the membrane surface.

2. The rate of colloidal fouling increases as the solution ionic strength and particle concentration in suspension increase. The increase in fouling rate in this case is attributed to the higher rate of particle deposition onto the membrane surface.

3. To better understand colloidal fouling of RO membranes, one should consider particle–membrane and particle–retained particle interactions. These interactions are controlled by

APPENDIX. REFERENCES

Adamczyk, Z., Siwek, B., Zembala, M., and Belouschek, P. (1994). "Kinetics of localized adsorption of colloid particles." *Adv. Colloid Interface Sci.*, 48, 151-280.

Altena, F.W., and Belfort, G. (1984). "Lateral migration of solid particles in Poiseuille flow." *Chem. Eng. Sci.*, 49, 343-355.

AWWA Membrane Technology Research Committee (1992). "Committee report: membrane processes in potable water treatment." *J. Am. Water Works Assoc.*, 84, 59-67.

Belfort, G. (1989). "Fluid mechanics in membrane filtration: Recent Developments." *J. Memb. Sci.*, 40, 123-147.

Brunelle, M. T. (1980). "Colloidal fouling of reverse osmosis membranes." *Desalination*, 32, 127-135.

Buros, O.K. (1989). "Desalting practices in the United States." *J. Am. Water Works Assoc.*, 81, 11-38.

Chellam, S., and Wiesner, M.R. (1992). "Particle transport in clean membrane filters in laminar flow." *Envir. Sci. Technol.*, 26, 1611-1621.

Clifford, D., Subramonia, S., and Sorg, T. J. (1986). "Removing dissolved inorganic contaminants from water." *Envir. Sci. Technol.*, 20, 1072-1080.

Cohen, R.D., and Probstein, R. F. (1986). "Colloidal fouling of reverse osmosis membranes." *J. Colloid Interface Sci.*, 114, 194-207.

Degussa Technical Bulletin (1990). "Highly dispersed metallic oxides produced by the Aerosol process." Technical Bulletin No. 56.

DiGiano, F.A, Braghetta, A., Nilson, J., and Utne, B. (1994). "Fouling of nanofiltration membranes by natural organic matter." Proceedings of the 1994 National Conference on Environmental Engineering, Boulder, Colorado, pages 320-328.

Elimelech, M. (1994a). "Effect of particle size on the kinetics of particle deposition under attractive double layer interactions." *J. Colloid Interface Sci.*, 164, 190-199.

Elimelech, M. (1994b). "Particle deposition on ideal collectors from dilute flowing suspensions: mathematical formulation, numerical solution, and simulations." *Sep. Technol.*, 4, 186-212.

Elimelech, M., Chen, W. H., and Waypa, J. J. (1994). "Measuring the zeta (electrokinetic) potential of reverse osmosis membranes by a streaming potential analyzer.", *Desalination*, 95, 269-286.

Fane, A.G., and Fell, C.J.D. (1987). "A review of fouling and fouling control in ultrafiltration." *Desalination*, 62, 117-136.

Gilron, J., and Hasson, D. (1987). "Calcium sulphate fouling of reverse osmosis membrane: flux decline mechanism." *Chem. Eng. Sci.*, 42, 2351-2360.

Song, L., and Elimelech, M. (1993). "Dynamics of colloid deposition in porous media: modeling the role of retained particles." *Colloids Surfaces A*, 73, 49-63.

Song, L., and Elimelech, M. (1994). To be submitted to: *J. Colloid Interface Sci.*.

Stone, A.T. (1989). "Enhanced rates of monophenyl terephthalate hydrolysis in aluminum oxide suspensions." *J. Colloid Interface Sci.*, 127, 429-441.

Stumm, W. (1992). *Chemistry of the Solid-Water Interface: Processes at the Mineral-Water and Particle-Water Interface in Natural Systems*. John Wiley & Sons, Inc., New York, NY.

Tiller, C.L., and O'Melia, C.R. (1993). "Natural organic matter and colloidal stability: models and measurements." *Colloids Surfaces A*, 73, 89-102.

Tipping E. and Higgins D.C. (1982). "The effect of adsorbed humic substances on the colloid stability of haematite particles." *Colloids Surfaces* 5, 85-92.

Verwey, E.J.W., and Overbeek, J.Th.G. (1948). *Theory of the stability of lyophobic colloids.* Elsevier, Amsterdam.

Walker, J.F., Wilson, J.H., and Brown, C.H. (1990). "Minimization of chromium-contaminated wastewater at a plating facility in the eastern United States." *Envir. Progr.*, 9, 156-160.

Wiesner, M. R., Clark, M.M., and Malleville, J. (1989). "Membrane filtration of coagulated suspension." *J. Envir. Engrg., ASCE*, 115, 20-40.

Winfield, B.A. (1979a). "The treatment of sewage effluents by reverse osmosis -pH based studies of the fouling layer and its removal." *Water Res.*, 13, 561-564.

Winfield, B.A. (1979b). "A study of the factors affecting the rate of fouling of reverse osmosis membranes treating secondary sewage effluents." *Water. Res.*, 13, 565-569.

Yokoyama, A., Srinivasan, K.R., and Fogler, H.S. (1989). "Stabilization mechanism by acidic polysacharides. Effects of electrostatic interactions on stability and stabilization." *Langmuir*, 5, 534-538.

KEY WORDS

Colloidal fouling

Membrane Fouling

Reverse osmosis

Colloids

Membrane technology

Desalination

Flux decline

Membrane Separation

Polymeric Membranes

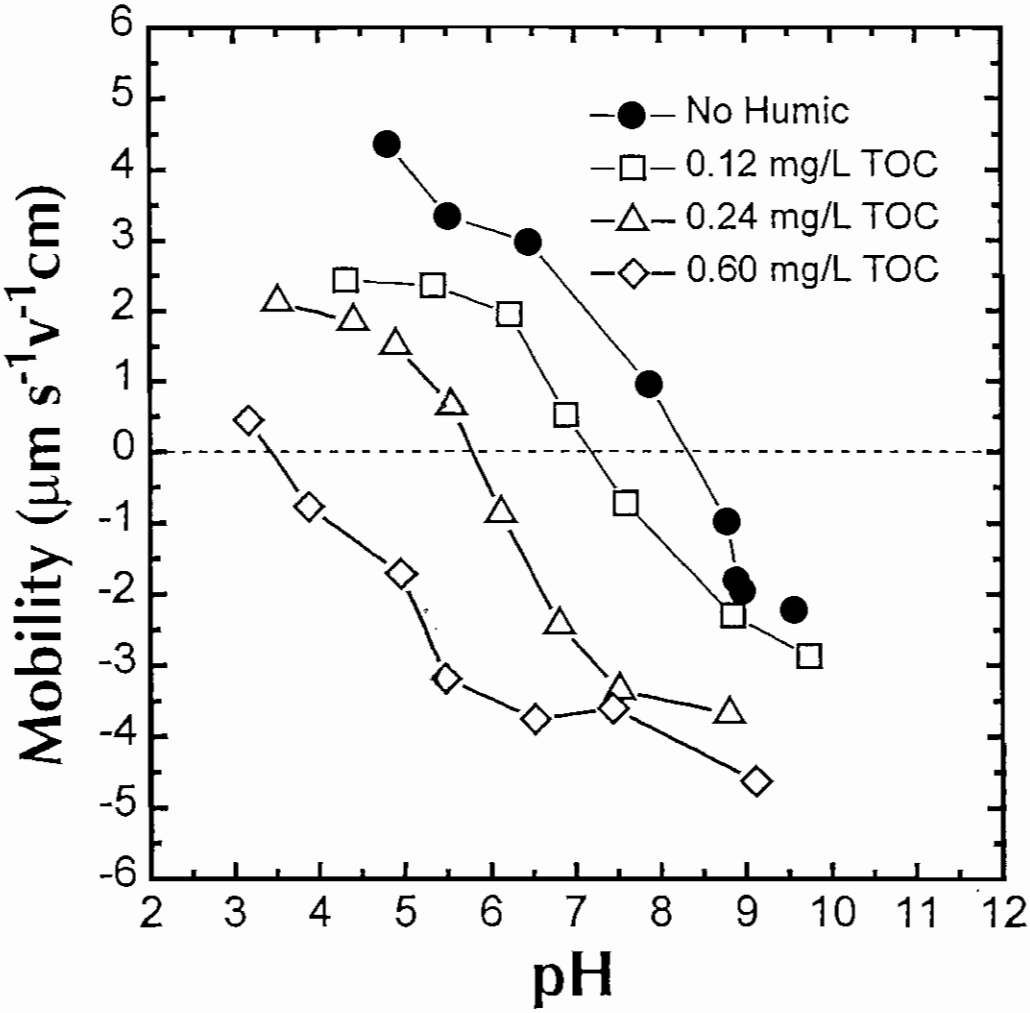
No Humic
0.12 mg/L TOC
0.24 mg/L TOC
0.60 mg/L TOC
Mobility (μm s-1v-1cm)
pH
6
5
4
3
2
1
0
-1
-2
-3
-4
-5
-6
2
3
4
5
6
7
8
9
10
11
12

Figure 2

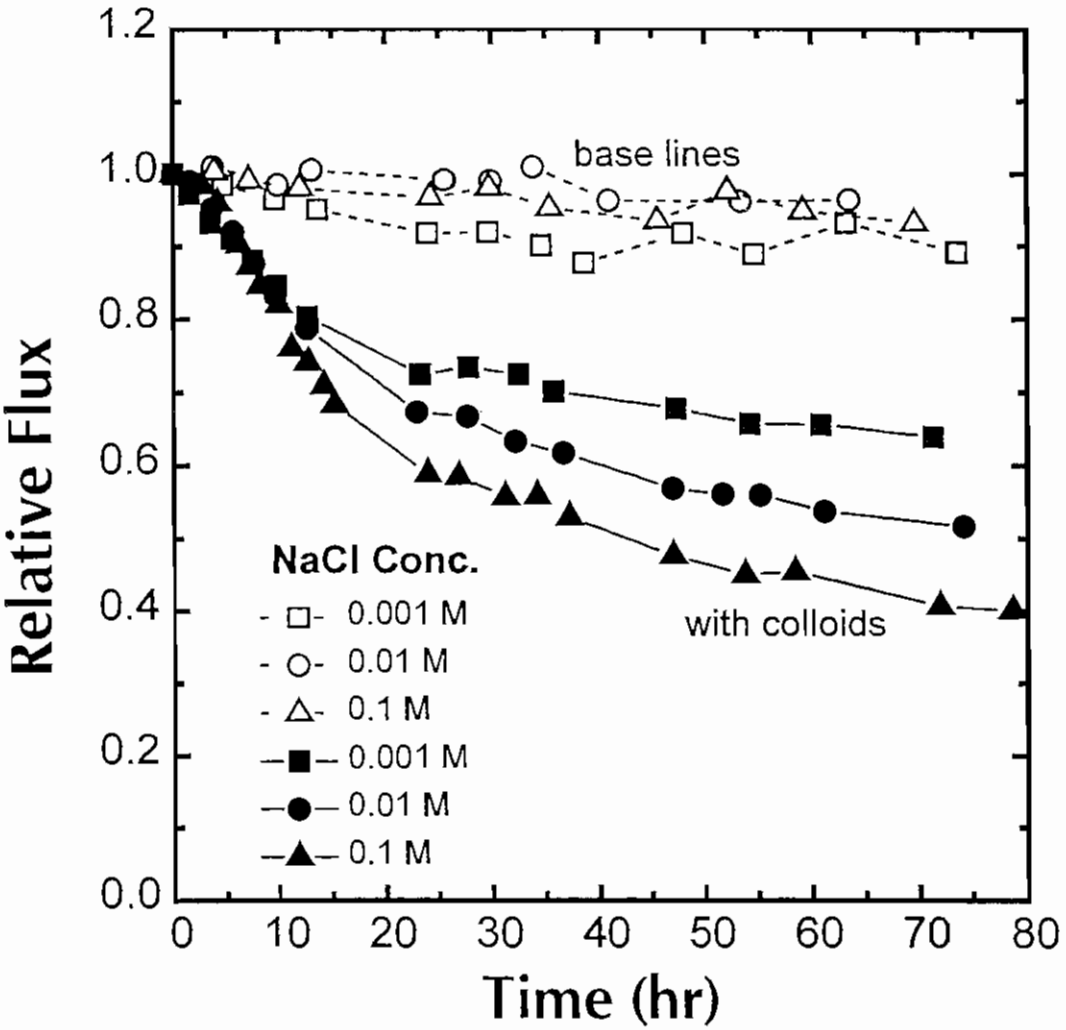
1.2
1.0
0.8
0.6
0.4
0.2
0.0
Relative Flux
0
10
20
30
40
50
60
70
80
Time (hr)
base lines
with colloids
NaCl Conc.
0.001 M
0.01 M
0.1 M
0.001 M
0.01 M
0.1 M

Figure 4

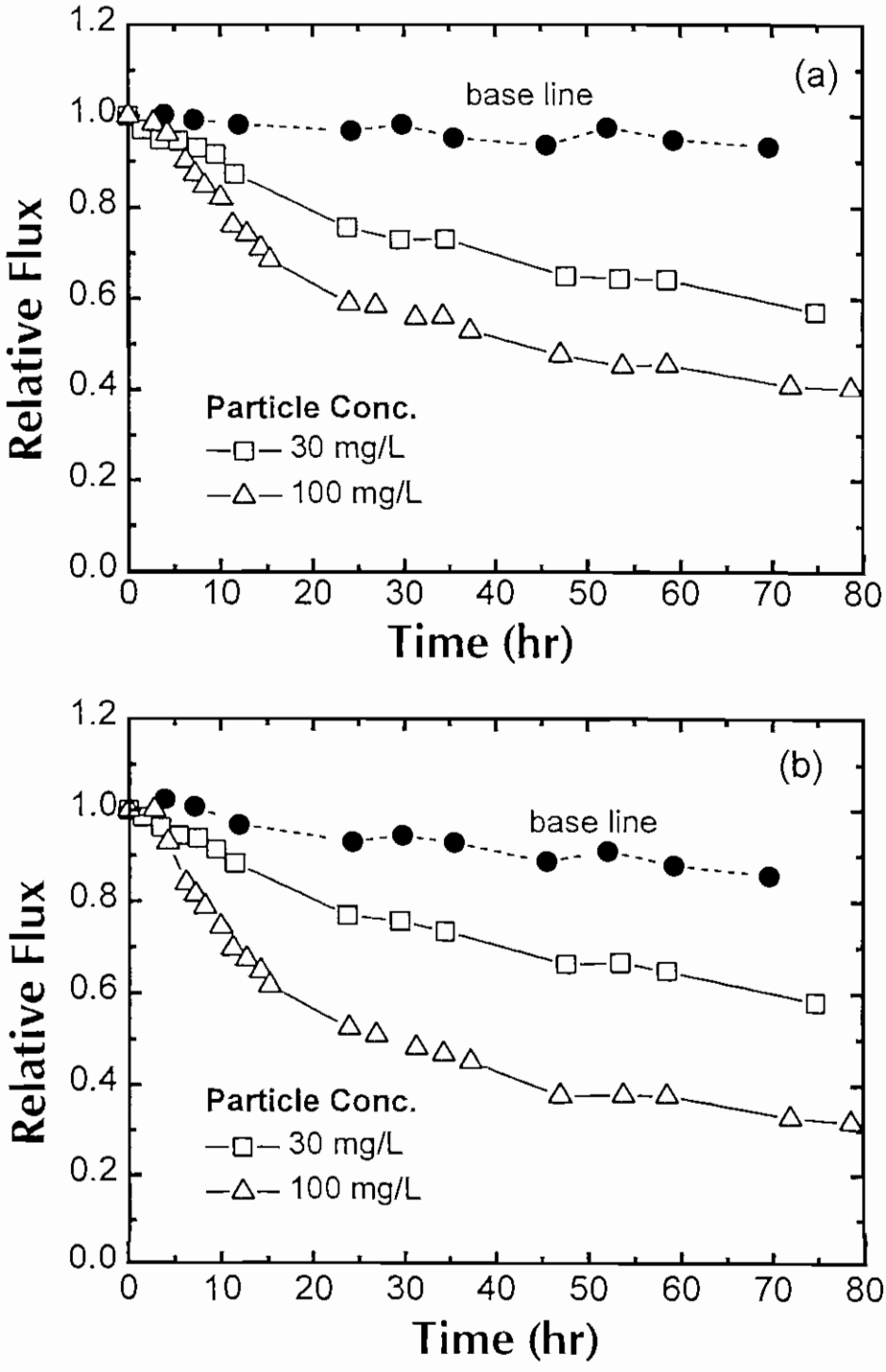
(a)
base line
Relative Flux
Time (hr)
Particle Conc.
30 mg/L
100 mg/L
(b)
base line
Relative Flux
Time (hr)
Particle Conc.
30 mg/L
100 mg/L

Figure 6

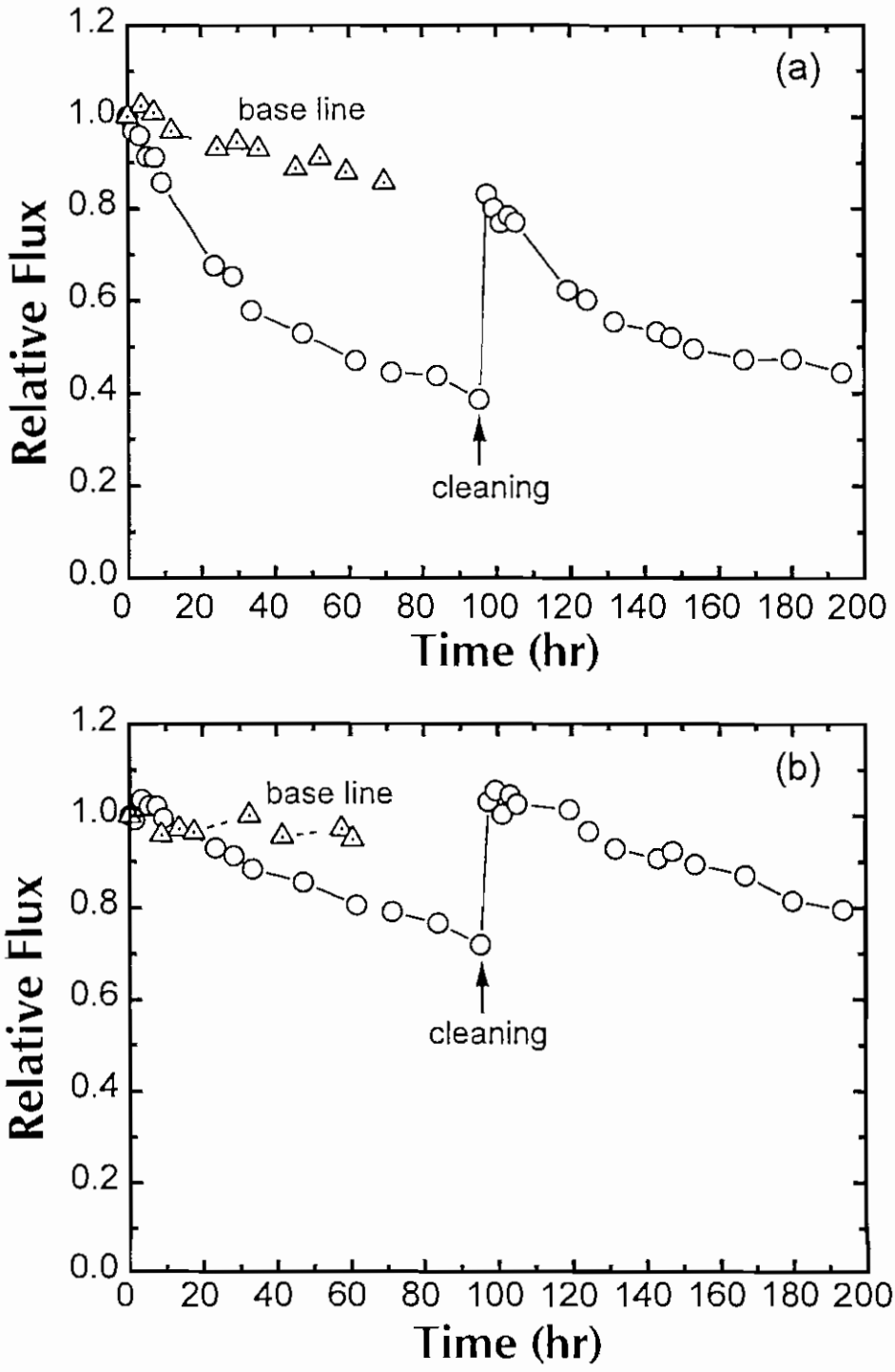
(a)
base line
cleaning
Relative Flux
Time (hr)
(b)
base line
cleaning
Relative Flux
Time (hr)

Figure 8

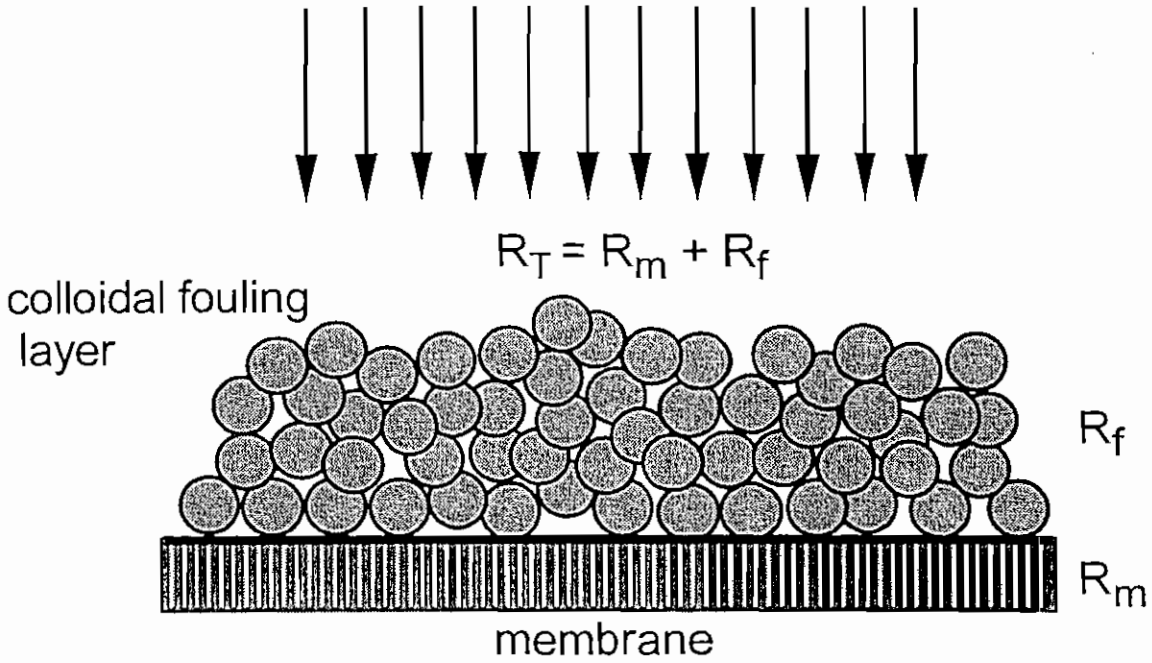

Figure 10

Appendix III

Song, L. and Elimelech, M. "Particle Deposition onto a Permeable Surface in laminar Flow", submitted to: ***Journal of Colloid and Interface Science***.

Particle Deposition onto a Permeable Surface in Laminar Flow

Journal of Colloid and Interface Science

Revised: December 20, 1994

by

Lianfa Song and Menachem Elimelech*

School of Engineering and Applied Science
4173 Engineering I
University of California
Los Angeles, CA 90024-1593

Tel: (310) 825-1774
Fax: (310) 206-2222
e-mail: elim@seas.ucla.edu

Running Title: *Particle Deposition onto a Permeable Surface*

---

* Author to whom all correspondence should be addressed.

Particle deposition onto stationary surfaces is a complex process where several particle transport and interaction mechanisms are involved. Over the past three decades, numerous investigations on the initial deposition rate of colloidal particles onto impermeable, solid surfaces have appeared in the literature (10-25). These studies have investigated and explained, at least semi-quantitatively, the effects of various physical and chemical factors on particle deposition kinetics. It is well established that particle deposition kinetics under unfavorable chemical conditions are controlled by the colloidal interactions between the particle and the surface; particle deposition rate is significantly reduced when repulsive double layer interactions predominate (11-13, 17, 21, 24).

Unlike deposition onto impermeable surfaces where the flow perpendicular to the surface vanishes as the separation distance approaches zero, the finite permeation rate through a permeable surface may provide an effective drag force for particles to overcome the repulsive colloidal forces and to deposit onto the permeable surface. Therefore, particle deposition kinetics onto permeable surfaces would no longer be controlled by colloidal interactions alone. A strong interplay between permeation drag and electrical double layer repulsion is expected.

Early works in this area concerned with the flow field in a channel bounded by permeable walls. Berman (26) was the first to provide a complete solution for the two-dimensional laminar flow field in a permeable, rectangular channel. In addition, experimental and theoretical investigations on the phenomenon of inertia-induced lift pointed out that this lateral transport mechanism is important for non-Brownian particles in a laminar shear flow over a surface (2, 27-30). Incorporation of Berman's flow field and theories for inertial lift provides the basis for trajectory analysis of particle transport over permeable surfaces. Trajectory analysis is a useful tool to investigate the deposition of large, non-Brownian particles from flowing suspensions onto stationary surfaces (31).

The first theoretical investigation of particle deposition onto permeable surfaces with the concept of trajectory analysis was carried out by Hung and Tien (6). In their analysis, Hung and Tien considered the effects of surface interactions (double layer and van der Waals), permeation drag, hydrodynamic (viscous) interaction, and gravitational force. Belfort and coworkers (2, 5, 29) later developed a trajectory model for particle transport in permeable channels of various geometries with consideration of inertial lift, permeation drag, and Berman's flow field. They further presented calculated trajectories of large, non-Brownian particles and the subsequent capture of particles by the permeable walls of the channel.

The trajectory studies discussed above are limited to large, non-Brownian particles. From a practical point of view, however, it is important to understand the deposition behavior of

Lagrangian equation leads to a Langevin-type equation, the solution of which results in stochastic trajectories (33, 36-38). Eulerian methods describe the concentration distribution of particles in time and space. For dilute suspensions of spherical particles, where interparticle interactions can be neglected, the concentration distribution of suspended particles is governed by the *convective diffusion equation.* In contrast to the Lagrangian approach, the difficulty of accounting for Brownian effects is eliminated when the Eulerian method is used.

2.1 The Convective Diffusion Equation

The convective diffusion equation in its general form is given by (34, 39)

$$\frac{\partial C}{\partial t} + \nabla \cdot \mathbf{J} = Q\,, \qquad [2.1]$$

where C is the particle number concentration, t is the time, $\mathbf{J}$ is the particle flux vector, and Q is a source or sink term. The particle flux vector is given by

$$\mathbf{J} = -\mathbf{D} \cdot \nabla C + \mathbf{u}C + \frac{\mathbf{D} \cdot \mathbf{F}}{kT} C\,. \qquad [2.2]$$

Here $\mathbf{D}$ is the particle diffusion tensor, $\mathbf{u}$ is the particle velocity induced by the flow of the suspending medium (*i.e.*, the fluid), k is the Boltzmann constant, T is the absolute temperature, and $\mathbf{F}$ is the external force vector. The terms on the right hand side of Eq. [2.2] describe the transport of particles induced by diffusion, fluid flow, and external forces, respectively.

Substituting Eq. [2.2] in [2.1] and assuming no source or sink terms reduce the convective diffusion equation to

$$\frac{\partial C}{\partial t} + \nabla \cdot (\mathbf{u}C) = \nabla \cdot (\mathbf{D} \cdot \nabla C) - \nabla \cdot \left(\frac{\mathbf{D} \cdot \mathbf{F}}{kT} C \right). \qquad [2.3]$$

Applications of this equation to particle coagulation (40) or deposition (41) show that a steady state is established after a relatively short period of time, which is much smaller than the time scales of interest in studying most particle deposition phenomena. Hence, Eq. [2.3] simplifies to the familiar steady state form:

$$\nabla \cdot (\mathbf{u}C) = \nabla \cdot (\mathbf{D} \cdot \nabla C) - \nabla \cdot \left(\frac{\mathbf{D} \cdot \mathbf{F}}{kT} C \right). \qquad [2.4]$$

This equation will be used in the analysis of particle deposition onto a permeable wall in a parallel plate channel as described in the following subsections.

2.3 Particle Lift Velocity

Particles in a laminar shear flow over a surface experience an inertia-induced lateral transport away from the surface; this transport mechanism is often termed *inertial lift*. Inertia-induced lateral migration of particles in a steady laminar flow was first observed by Segré and Silberberg (27, 28) and has since been investigated theoretically by numerous investigators. Cox and Brenner (46) were the first to analyze theoretically the complete problem of a particle in a shear flow near an impermeable wall, but their solutions were general in the form of integral functions. Following the theoretical approach of Cox and Brenner, Ho and Leal (47) and Vasseur and Cox (48) derived solutions for the lift velocity of a spherical particle in a slow, two-dimensional shear flow. Their equation for the lift velocity of a rigid, neutrally buoyant, freely rotating particle in a plane Poiseuille flow is given by

$$u_L = \frac{9}{4} V_0^2 \frac{a_p^3}{\nu B^2} \left(1 - \frac{V_w}{V_0} \frac{x}{B}\right)^2 g_2(\beta) \qquad [2.8]$$

where a_p is the particle radius and $g_2(\beta)$ is a complex function of the variable β that can be calculated numerically (47, 48). Belfort and coworkers (2, 5) have shown that the above equation is also valid for the problem of laminar flow over a surface with low permeability (e.g., ultrafiltration and reverse osmosis membranes). They further provided a polynomial fit for the function $g_2(\beta)$ by carrying out numerical calculations of the expressions provided by Vasseur and Cox (48):

$$\begin{aligned} g_2(\beta) = {} & 1.532139 - 12.182786\beta + 21.652283\beta^2 + 4.495068\beta^3 \\ & - 28.176666\beta^4 + 10.950694\beta^5 + 0.198042\beta^6 \end{aligned} \qquad [2.9]$$

The analysis described above is valid for slow flows where the Reynolds number based on the particle radius, Re_p, or the channel width, Re_c, is much smaller than unity, *i.e.*,

$$Re_p = \frac{V_0 a_p}{\nu} << 1 \qquad [2.10]$$

$$Re_c = \frac{V_0 B}{\nu} << 1 \qquad [2.11]$$

In addition, it was assumed in the theoretical derivation that the particle is not too close to the wall. Extensions of the theory to higher Reynolds numbers have been made by Schonberg and Hinch (49) and Drew et al. (50), who showed that at higher Reynolds numbers the inertia-

$$\mathbf{J_D} = -\mathbf{D} \cdot \nabla C \qquad [2.18]$$

where $\mathbf{J_D}$ is the diffusive flux vector and $\mathbf{D}$ is the particle diffusion tensor. The latter can be defined as (34)

$$\mathbf{D} = \mathbf{m}kT\,. \qquad [2.19]$$

where k is the Boltzmann constant, T is the absolute temperature, and $\mathbf{m}$ is the particle mobility tensor. For a spherical particle in an unbounded dilute suspension, the mobility is isotropic and is given by

$$m = \frac{1}{6\pi\mu a_p}\,, \qquad [2.20]$$

and the diffusion coefficient is given by the well-known Stokes-Einstein equation:

$$D_\infty = \frac{kT}{6\pi\mu a_p}\,. \qquad [2.21]$$

In the vicinity of a solid surface, however, the mobility of particles changes due to hydrodynamic interaction. In this case, the perpendicular and tangent mobility tensor components, respectively, are given by (16, 17)

$$m_{\perp} = \frac{f_1}{6\pi\mu a_p} \qquad [2.22]$$

$$m_{//} = \frac{f_4}{6\pi\mu a_p}\,, \qquad [2.23]$$

where f_1 and f_4 are universal correction factors for hydrodynamic interaction (52, 53). Combining Eqs. [2.19] and [2.21]-[2.23] results in the perpendicular and parallel (tangent) components of the diffusion tensor, that is

$$D_{\perp} = f_1 D_\infty \qquad [2.24]$$

$$D_{//} = f_4 D_\infty\,. \qquad [2.25]$$

2.6 External Forces

In most problems of particle deposition in liquids, the external forces are colloidal and gravitational, i.e.,

$$\mathbf{F} = \mathbf{F}_{\text{col}} + \mathbf{F}_G \qquad [2.26]$$

$$x^* = \frac{x}{L} \qquad [2.33]$$

$$\gamma = \frac{a_p}{B} \qquad [2.34]$$

$$B^* = \frac{B}{L} \qquad [2.35]$$

$$\Phi = \frac{\phi_T}{kT} \qquad [2.36]$$

$$Pe = \frac{V_0 a_p}{D_\infty} \qquad [2.37]$$

$$Pe_w = \frac{V_w a_p}{D_\infty} \qquad [2.38]$$

$$F_G^* = \frac{F_G a_p}{kT} \qquad [2.39]$$

With the use of these variables and the various expressions for the particle flow field described earlier, the convective diffusion equation in a rectangular coordinate system can be written in dimensionless form as

$$\begin{aligned} & Pe\gamma\,\xi\, f_3\, B^* \frac{dg_1(\beta)}{d\beta}\frac{\partial C^*}{\partial x^*} \\ & = f_1 \frac{\partial^2 C^*}{\partial H^2} \\ & + \left\{\frac{\partial f_1}{\partial H} + f_1\left(\frac{\partial \Phi}{\partial H} - F_G^*\right) - \left[Pe_w g_1(\beta) + Pe\Gamma\xi^2 g_2(\beta)\right]\right\}\frac{\partial C^*}{\partial H} \\ & + \left\{f_1\frac{\partial^2 \Phi}{\partial H^2} + \frac{\partial f_1}{\partial H}\left(\frac{\partial \Phi}{\partial H} - F_G^*\right) - \left[(1-f_3)Pe_w\gamma\frac{dg_1(\beta)}{d\beta} + Pe\gamma\,\Gamma\xi^2\frac{dg_2(\beta)}{d\beta}\right]\right\}C^* \end{aligned} \qquad [2.40]$$

In the derivation of this equation, the following assumptions were made: (i) colloidal forces act perpendicular to the permeable wall, (ii) particle diffusive flux tangent to the permeable wall is much smaller than the perpendicular component, and (iii) the channel is horizontal so that the gravitational force acts perpendicular to the permeable surface.

For convenience in numerical calculations, Eq. [2.40] can be written as

$$b_0\frac{\partial C^*}{\partial x^*} = b_1\frac{\partial^2 C^*}{\partial H^2} + b_2\frac{\partial C^*}{\partial H} + b_3 C^* \qquad [2.41]$$

particles due to the action of external forces (colloidal and gravitational). Hence, the overall dimensionless particle flux to the collector surface can be written as

$$Sh = Sh_{\mathrm{D}} + Sh_{P} + Sh_{\mathrm{L}} + Sh_{\mathrm{Ex}} \qquad [2.45]$$

where Sh_{D}, Sh_{P}, Sh_{L}, and Sh_{Ex} are the particle flux components due to diffusion, permeation, inertial lift, and external forces, respectively, as described in Eq. [2.44].

Since the Sherwood number, by definition, is related to particle size ($Sh \propto J a_p^2$), its use in investigations on the effect of particle size in particle deposition is not recommended. In such investigations, we use a local particle transfer rate, K, defined as

$$K = \frac{ShD_{\infty}}{a_p} \qquad [2.46]$$

The overall particle deposition rate at the permeable surface can be calculated from the local deposition rate at the permeable wall (i.e., at H=0). Hence, the average Sherwood number, Sh^*, is simply

$$Sh^* = \frac{1}{L}\int_0^L Sh\big|_{H\to 0}\, dx \qquad [2.47]$$

where L is the length of the channel. Furthermore, an average particle transfer rate, K^*, may be used. This is defined as

$$K^* = \frac{Sh^* D_{\infty}}{a_p} \qquad [2.48]$$

3. NUMERICAL SOLUTION

No analytical solutions exist for the convective diffusion equation when colloidal and hydrodynamic interactions are rigorously incorporated. A numerical solution can be obtained by using a modified Crank-Nicholson scheme with a non-uniform mesh (32, 58, 59). It has been shown that for unfavorable deposition (*i.e.*, when repulsive double layer interactions predominate), the convective diffusion equation becomes a stiff problem with turning points (39). A numerical procedure, previously developed for particle deposition onto a spherical collector, is adapted to our problem to overcome the numerical difficulties associated with stiff problems with turning points (39). The principles of this numerical procedure are outlined below.

where c_1 is a constant. Equation [3.3] implies that the change of the dimensionless colloidal interaction potential Φ in each step should be kept less than 1 to maintain stability of the numerical solution.

The second requirement for a stable numerical solution is to allocate sufficient grid points around the turning point. This requirement is met by maintaining the following criterion:

$$\left|\Delta\left(\frac{d\Phi}{dH}\right)\right| < c_2 \le 10^{-3} \max_{i,j}\left[\left(\frac{d\Phi}{dH}\right)_i - \left(\frac{d\Phi}{dH}\right)_j\right] \qquad \text{when} \quad \frac{d^2\Phi}{dH^2} > 0 \qquad [3.4]$$

where c_2 is another constant. As will be shown in the next subsection, if this operational criterion is satisfied, enough mesh points will be allocated in the region near the turning points.

For large particles, turning points can also result from changes in the inertia-induced lift velocity. In this case, a similar procedure is used to allocate sufficient grid points in the region of these turning points.

3.3 Allocation of Mesh Grids

The strategy for mesh grids allocation is to first build an initial mesh and then add more grids where the above operational criteria are not satisfied. Since the domain for H in the channel can be as large as 10^6 and only a few thousands steps are used, a uniform initial mesh cannot be used. If a uniform mesh were used, the step size might be several hundreds times of the particle size. In this case, all the information on colloidal interactions would be lost because the colloidal interactions change dramatically around the energy barrier over a distance of a few nanometers. Consequently, we divide the H domain into several regions. The length of the most inner region is selected as H=10, and the length of the subsequent regions increases by a factor of 10 (i.e., the second region is 100, the third is 1000, and so on). The number of regions is so determined that the whole domain is covered. The initial mesh is made by dividing each region into 1000 equal steps. After the initial mesh is set, the following procedure is used to allocate additional mesh points:

(a) The total colloidal interaction potential and its first and second derivatives are calculated for each point.

(b) New mesh points are inserted uniformly between adjacent mesh points if any of the above operational criteria (*i.e.*, Eqs. [3.3] and [3.4]) is not satisfied. The number of points inserted, N, is determined by

$$N = \max\left(2\left|\Delta\Phi\right|/c_1,\quad 2\left|\Delta\left(\frac{d\Phi}{dH}\right)\right|/c_2\right) \qquad [3.5]$$

dependent on particle size. The local *Sh* and *K* as a function of the dimensionless axial location on the permeable surface, $x^*=x/L$, are presented in Fig. 2. These simulations were carried out for neutrally buoyant particles of different sizes, ranging from 10 nm to 3 μm in diameter. For simplicity, the particles and the permeable surface are assumed to be neutrally charged in the simulations presented in Fig. 2. Furthermore, the permeation velocity used is very small, so that particle transport and deposition are not dominated by permeation drag.

The simulations demonstrate that, for Brownian particles (*i.e.*, particles smaller than about 1 μm), the local *Sh* and *K* decrease along the channel according to $\sim x^{-1/3}$. This dependence is in accord with theoretical studies of colloid or mass transfer to impermeable surfaces when convective diffusion dominates (59, 61, 62). In this case, the decrease in particle deposition rate along the channel correlates with the increase in the thickness of the diffusion boundary layer as x increases (62). It is further shown that the transfer (deposition) rate of Brownian particles increases as the particle size decreases. This is because of the more efficient diffusive transport of smaller particles. The latter effect cannot be seen clearly from the local *Sh* (Fig. 2a) because by definition *Sh* is a function of particle size ($Sh \equiv J_\perp a_p/D_\infty$, *i.e.*, $Sh \propto a_p^2 J_\perp$). For particles larger than 1 μm, the local deposition rate becomes smaller and declines faster along the channel compared to the case with smaller particles. This behavior points out that back transport by inertial lift is significant for the large particles. As the particle size increases, the inertial lift increases, thus reducing the particle transfer rate to the permeable surface.

The results shown in Fig. 2 clearly demonstrate that particle size plays an important role in particle deposition onto permeable surfaces. It is further shown that the use of *Sh* for quantifying the deposition rate is not suitable for studies on the effect of particle size because of its complex dependence on particle radius. In investigations on the role of particle size in particle deposition, it is advantageous to use the particle transfer rate *K* (as in Fig. 2b).

Additional simulations for the effect of particle size on the particle deposition rate are shown in Fig. 3. The simulations for the average particle transfer rate, K^*, are shown for three permeation velocities (V_w=10^{-5}, 10^{-7}, and 10^{-9} m/s). At low permeation velocities (10^{-7} and 10^{-9} m/s), the average particle transfer rate decreases with an increase in particle size. The decrease in the average particle transfer rate is moderate up to a particle size of about 2 μm, beyond which a sharp decrease in the deposition rate is observed. The decrease in deposition rate in the first region (i.e., below 2 μm) is attributed to the decrease in the diffusive transport as particle size increases. In the second region (*i.e.*, above 2 μm), the sharp decrease in the deposition rate results from the effect of inertial lift. Inertial lift induces back transport of particles away from the membrane and thus reduces significantly the particle deposition rate. One should note that based on Eq. [2.8], the inertia-induced particle velocity is highly dependent on particle size ($u_L \propto a_p^3$).

be seen from the results in Fig. 5 that particle deposition is very sensitive to changes in solution ionic strength. For instance, particle deposition rate increases by more than three orders of magnitude as the ionic strength increases from 0.001 to 0.006 M.

An interesting observation in Fig. 5 is that the local particle deposition rate increases along the channel in the entrance region. This behavior is in contrast to that observed in deposition of Brownian particles in the absence of double layer interactions. In the latter case, the local deposition rate decreases along the permeable wall of the channel (see Fig. 2). The behavior observed in Fig. 5 can be explained by the interplay between the permeation drag and the repulsive double layer force. Because the energy barrier hinders particle deposition, particles transported by permeation drag toward the permeable surface accumulate before the energy barrier and form a sharp concentration front. Some of the particles then penetrate the energy barrier by diffusion and deposit onto the permeable surface. At the channel inlet, there is no particle accumulation before the energy barrier. As the suspension flows through the channel, particles accumulate before the energy barrier and the deposition rate increases because of the increase in diffusional transport over the energy barrier. Eventually, an equilibrium is reached when the rate of particle transport by permeation drag to the front of the energy barrier is balanced by back diffusion of particles to the bulk suspension. This equilibrium stage is represented by the horizontal segments of the deposition rate curves shown in Fig. 5.

In the above hypothesis, permeation velocity plays an important role in determining the behavior of the local particle deposition rate, because it provides the primary transport mechanism for particles that accumulate in front of the energy barrier. According to this supposition, the local particle deposition rate would not increase along the channel if the permeation rate is sufficiently small. To verify our proposed mechanism on the interplay between electrical double layer interaction and permeation flow, calculations of particle deposition at an extremely small permeation velocity (10^{-11} m/s) have been carried out (Fig. 6). As shown, the local particle deposition rate decreases continuously along the channel, albeit to a small extent, for all ionic strengths. In this case, particles do not accumulate in front of the energy barrier because transport by permeation drag is negligible. The much more moderate decline of the local particle deposition rate along the channel in Fig. 6, compared to deposition in the absence of double layer repulsion (Fig. 2), is an indirect evidence that double layer interaction influences the behavior of the local deposition rate.

4.3 Effect of Permeation Velocity on Particle Deposition

As shown in the previous section, permeation velocity has a marked effect on the magnitude and the local behavior of particle deposition onto a permeable surface. The effect of

Figure 9 presents the local *Sh* of Brownian particles for various cross-flow velocities and at two permeation rates (10^{-5} and 10^{-7} m/s). When the permeation velocity is 10^{-5} m/s, particle deposition rate is primarily controlled by permeation drag, and hence, the cross-flow velocity has a small effect on the deposition rate. The particle deposition rate increases only slightly despite the two orders of magnitude increase of the cross-flow velocity. On the other hand, when the permeation velocity is low, particle deposition is controlled by diffusion, and the effect of cross-flow velocity on particle deposition rate is much more pronounced. Nonetheless, the increase in deposition rate in the later case is by less than one order of magnitude for two orders of magnitude increase in the cross-flow velocity. It is therefore concluded that the influence of cross-flow velocity on the initial deposition rate of Brownian particles onto permeable surfaces is rather limited.

For large, non-Brownian particles, the deposition behavior is quite different than that of small, Brownian particles because of the effect of inertial lift. Figure 10 presents the local *Sh* of 3-μm particles for various cross-flow velocities and at two permeation rates (10^{-5} and 10^{-7} m/s). As shown, deposition rate of non-Brownian particles decreases with increasing cross velocity, in contrast to the increase in deposition rate with cross-flow velocity for Brownian particles (Fig. 9). It is further shown that the deposition rate of non-Brownian particles is very sensitive to cross-flow velocity, in particular at low permeation rates. For example, Fig. 10b shows that increasing the cross-flow velocity from 0.10 to 0.15 m/s results in a decrease of the local *Sh* by several orders of magnitude.

Another interesting observation is the behavior of the local deposition rate of non-Brownian particles at various cross-flow velocities and permeation rates. When the permeation velocity is 10^{-5} m/s (Fig. 10a), the local deposition rate increases along the channel for most cross-flow velocities. This observation indicates that, under these conditions, the transport of particles toward the surface by permeation drag can be larger than the back transport of particles away from the surface by inertial lift. At low permeation velocity (Fig. 10b), the decrease in the local deposition rate along the channel indicates that back transport by inertial lift is much larger than transport by permeation drag.

In addition to its marked dependence on particle size, inertial lift is also dependent on the cross-flow velocity (based on Eq. [2.8], $u_L \propto V_0^2$). The dependence of the average deposition rate, expressed as *Sh**, on the cross-flow velocity of 3-μm particles at three different permeation velocities is shown in Fig. 11. At a very low permeation rate (10^{-9} m/s), the particle deposition rate first increases with increasing the cross-flow velocity and then decreases above a certain cross-flow. The increase in cross-flow velocity reduces the thickness of the diffusion boundary layer which results in increased particle transfer rate. As the cross-flow velocity increases, the inertial lift becomes significant and the deposition rate decreases. At higher permeation

force develops which may significantly reduced particle deposition, especially at low permeation rates. Hence, to demonstrate the importance of inertial lift in particle transport, electrical double layer interaction was not considered here. It is shown in Fig. 13 that permeation drag and inertial lift are the two dominant flux components in almost the entire width of the channel, and the total particle transport rate is roughly the algebraic sum of these two fluxes. The attractive van der Waals interaction contributes to the overall particle flux only in a very small region near the permeable surface. Particle diffusion is negligible for the entire range because (i) diffusive transport is not significant for large particles and (ii) there is no repulsive energy barrier to induce particle accumulation in front of the barrier.

5. CONCLUSION

Particle deposition onto a permeable surface under laminar flow conditions is determined by a complex interplay between several transport and interaction mechanisms. A numerical solution of the rigorously formulated convective diffusion equation provides a powerful tool for investigating this problem.

Our theoretical investigation shows that the rate of particle deposition is strongly dependent on particle size. For neutrally buoyant particles, the initial deposition rate decreases continuously as particle size increases. There exists a critical particle size, for a given set of chemical and physical conditions, beyond which the deposition rate drops abruptly to an extremely small value. This sharp decrease in deposition rate is attributed to the inertia-induced lift force.

Under conditions where inertial lift is negligible, the interplay between double layer interaction and permeation drag becomes significant. At large permeation rates, the deposition rate is dominated by permeation drag, while for small permeation rates diffusive transport and repulsive double layer interaction play an important role.

It is apparent from the results presented in this paper that permeation velocity is a very important parameter that controls particle deposition onto permeable surfaces. Permeation velocity not only influences the magnitude of the average particle deposition rate, but it also controls the pattern of particle deposition along the channel. Hence, reducing the permeation velocity through low permeability membranes, such as reverse osmosis and ultrafiltration, can minimize the fouling of these membranes by colloidal particles.

REFERENCES

1. Clark, A. T., Jones, R. B., and Lal, M., *Colloids Surf.*, **44**, 315 (1990).
2. Altena, F. W., and Belfort, G., *Chem. Eng. Sci.*, **39**, 343 (1984).
3. Chellam, S., and Wiesner, M. R., *Environ. Sci. Technol.*, **26**, 1611 (1992).
4. Sherwood, J. D., *PhysicoChem. Hydrodyn.*, **10**, 3 (1988).
5. Belfort, G., *J. Memb. Sci.*, **35**, 245 (1988).
6. Hung, C.-C., and Tien, C., *Desalination*, **18**, 173 (1976).
7. Elimelech, M., Chen, W. H., and Waypa, J. J., *Desalination*, **95**, 269 (1994).
8. Potts, D. E., Ahlert, R. C., and Wang, S. S., *Desalination*, **36**, 235 (1981).
9. Cohen, R. D., and Probstein, R. F., *J. Colloid Interface Sci.* **114**, 194 (1986).
10. Adamczyk, Z., *Colloids Surf.*, **35**, 283 (1989).
11. Bowen, B. D., and Epstein, N., *J. Colloid Interface Sci.*, **72**, 81 (1979).
12. Elimelech, M., and. O'Melia, C. R., *Langmuir*, **6**, 1153 (1990).
13. Vaidyanathan, R., and Tien, C., *Chem. Eng. Sci.* **46**, 967 (1991).
14. Chari, K., and Rajagopalan, R., *J. Chem. Soc. Faraday Trans. 2* **81**, 1345 (1985).
15. Elimelech, M., *J. Colloid Interface Sci.* **146**, 337 (1991)
16. Jia, X. and Williams, R.A., *Chem. Eng. Comm.*, **91**, 127 (1990).
17. Adamczyk, Z., Czarnecki, J., Dabros, J., and van de Ven T. G. M., *Adv. Colloid Interface Sci.* **19**, 183 (1983).
18. Prieve, D. C., and Ruckenstein, E., *AIChE J.* **20**, 1178 (1974).
19. Elimelech, M., and Song, L., *Sep. Technol*, **2**, 2, (1992).
20. Shapiro, M., Brenner, H., and Guell, D.C., *J. Colloid Interface Sci.*, **136**, 552 (1990).
21. Ruckenstein, E., and Prieve, D. C., *J. Chem. Soc., Faraday Trans. 2* **69**, 1522 (1973).
22. Spielman, L. A., *Ann. Rev. Fluid Mech.*, **9**, 297 (1977).
23. Elimelech, M., *J. Colloid Interface Sci.*, **164**, 81 (1994).
24. Spielman, L. A., and Friedlander, S. K., *J. Colloid Interface Sci.* **46**, 22 (1974).
25. Bowen, B. D., Levine, S., and Epstein, N., *J. Colloid Interface Sci.*, **72**, 81 (1976).
26. Berman, A. S., *J. Appl. Phys.*, **24**, 1232 (1953).
27. Segré, G., and Silberberg, A., *Nature*, **189**, 209 (1961).

52. Brenner, H., *Chem. Eng. Sci.* **16**, 242 (1961).

53. Goldman, A. J., Cox, R. G., and Brenner, H., *Chem. Eng. Sci.* **22**, 637 (1967).

54. Derjaguin, B. V., and Landau, L. D., *Acta Physicochim. URSS* **14**, 633 (1941).

55. Verwey, E. J. W., and Overbeek J. Th. G., "Theory of the Stability of Lyophobic Colloids.", Elsevier, Amsterdam, 1948.

56. Gregory, J., *J. Colloid Interface Sci.* **83**, 138 (1981).

57. Hogg, R., Healy, T. W., and Fuerstenau, D. W. *Trans. Faraday Soc.* **62**, 1638 (1966).

58. Elimelech, M., and Song, L., *in* "Transport and Remediation of Subsurface Environments: Colloidal, Interfacial, and Surfactant Phenomena", (D. A. Sabatini and R. C. Knox Editors), Chapter 3, pp. 26-39, ACS Symposium Series 491, American Chemical Society, Washington, D. C., 1992.

59. Adamczyk, Z., and van de Ven, T. G. M., *J. Colloid Interface Sci.*, **80**, 340 (1981).

60. Pearson, C. E. *J. Math. Phys.* 1967, **47**, 134.

61. Levich, V. G. "Physicochemical Hydrodynamics." Prentice Hall, New Jersey, 1962.

62. Cussler, E. L. "Diffusion: Mass Transfer in Fluid Systems", Cambridge University Press, Cambridge, UK, 1984.

K^*	average particle transfer rate defined by Eq. [2.48]
k	Boltzmann constant, 1.3805×10^{-23} J/°K
L	channel length
$\mathbf{m}$	particle mobility tensor
m	particle mobility in an infinite (unbounded) medium
$m_{\perp}$	perpendicular component of the particle mobility tensor
$m_{//}$	parallel component of the particle mobility tensor
N	number of points inserted between two adjacent grids defined by Eq. [3.5]
n	number of grid points used in the smoothing procedure of Eq. [3.6]
Q	source or sink term used in Eq. [2.1]
Pe	particle Peclet number defined by Eq. [2.37]
Pe_w	particle Peclet number defined by Eq. [2.38]
Re_c	channel Reynolds number defined by Eq. [2.11]
Re_p	particle Reynolds number defined by Eq. [2.10]
Re_w	wall Reynolds number defined as $V_w B/\nu$
Sh	local Sherwood number
Sh^*	average Sherwood number defined by Eq. [2.47]
Sh_i	various components of the local Sherwood number given by [2.45]
t	time
T	absolute temperature
V_0	average cross-flow velocity at the inlet of the channel (volumetric flow divided by the inlet section area)
V_w	permeation velocity
v_x	axial fluid velocity given by Eq. [2.5]
v_y	transverse fluid velocity given by Eq. [2.6]
$\mathbf{u}$	particle velocity vector
u_L	particle lift velocity
u_t	total particle velocity used in Eq. [3.1]
u_x	axial particle velocity given by Eq. [2.16]
u_y	transverse particle velocity given by Eq. [2.17]
x	spatial (axial) coordinate along the channel
x^*	dimensionless spatial coordinate along the channel; $x^*=x/L$
y	transverse coordinate, and distance from the impermeable surface to particle center

FIGURE CAPTIONS

FIG. 1. Schematic diagram of a parallel-plate channel with one permeable wall.

FIG. 2. (a) Local *Sh* as a function of the dimensionless longitudinal distance x^* for various particle sizes. (b) Local particle transfer rate K as a function of the dimensionless distance x^* for various particle sizes. The curves correspond to the following particle diameters: (1) 3.0, (2) 2.5, (3) 2.0, (4) 1.0, (5) 0.1, and (6) 0.01 μm. The other parameters used in the numerical calculations: V_0=0.1 m/s, V_w=10^{-7} m/s, L=0.5 m, B=1 mm, temp.=20°C, A=10^{-20} J, Δρ=0, and no electrical double layer interaction.

FIG. 3. The dependence of the average particle transfer rate K^* on particle size at three different permeation velocities (V_w). Numerical calculations were carried out with: V_0=0.1 m/s, L=0.5 m, B=1 mm, temp.=20°C, A=10^{-20} J, Δρ=0, and no electrical double layer interaction.

FIG. 4. The dependence of the average particle transfer rate K^* on particle size for particles of various densities. Particle densities in g/cm^3 are indicated next to each curve. The other parameters used in the numerical calculations: V_0=0.1 m/s, V_w=10^{-9} m/s, L=0.5 m, B=1 mm, temp.=20°C, A=10^{-20} J, and no electrical double layer interaction.

FIG. 5. The local *Sh* as a function of the dimensionless longitudinal distance x^* for various ionic strengths. The ionic strengths of 1:1 electrolyte are indicated next to each curve. The other parameters used in the numerical calculations: d_p=0.1 μm, V_0=0.1 m/s, V_w=10^{-5} m/s, L=0.5 m, B=1 mm, temp.=20°C, A=10^{-20} J, Δρ=0, ψ_1=-20 mV, and ψ_2=-25 mV.

FIG. 6. The local *Sh* as a function of the dimensionless longitudinal distance x^* for various ionic strengths. The ionic strengths of 1:1 electrolyte are indicated next to each curve. Numerical calculations were carried out for V_w=10^{-11} m/s. The other parameters are similar to those used in Fig. 5.

FIG. 7. The local *Sh* as a function of the dimensionless longitudinal distance x^* for various permeation velocities. Permeation velocities are indicated next to each curve. The other parameters used in the numerical calculations: d_p=0.1 μm, V_0=0.1 m/s, L=0.5 m, B=1 mm, temp.=20°C, A=10^{-20} J, Δρ=0, ψ_1=-20 mV, ψ_2=-25 mV, and ionic strength=5×10^{-3} M.

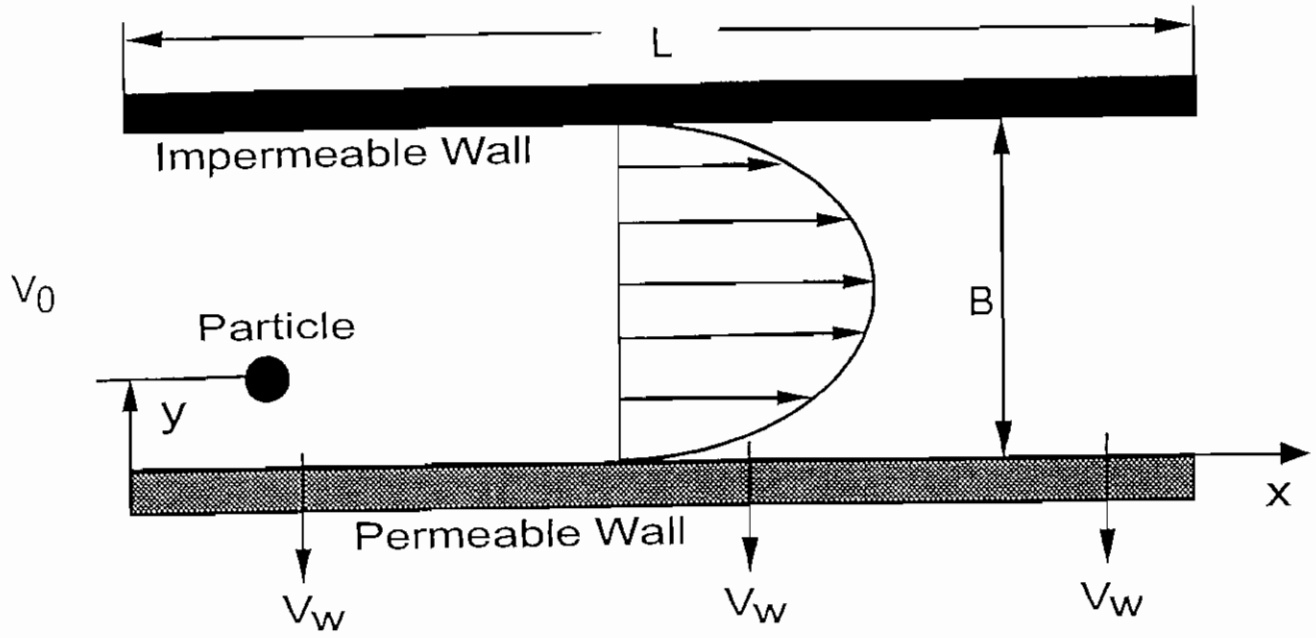

Figure 1

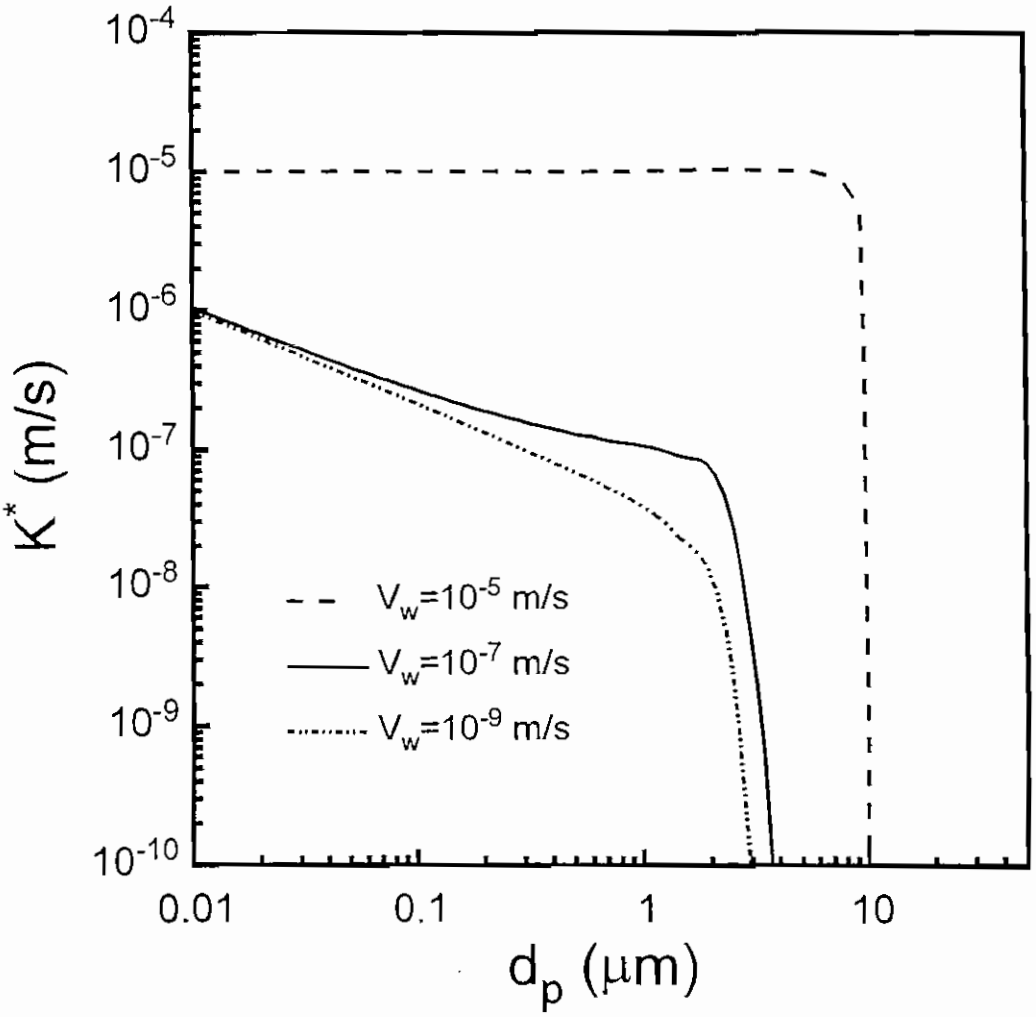
10^{-4}
10^{-5}
10^{-6}
10^{-7}
10^{-8}
10^{-9}
10^{-10}
K^* (m/s)
$V_w=10^{-5}$ m/s
$V_w=10^{-7}$ m/s
$V_w=10^{-9}$ m/s
0.01
0.1
1
10
d_p (μm)

Figure 3

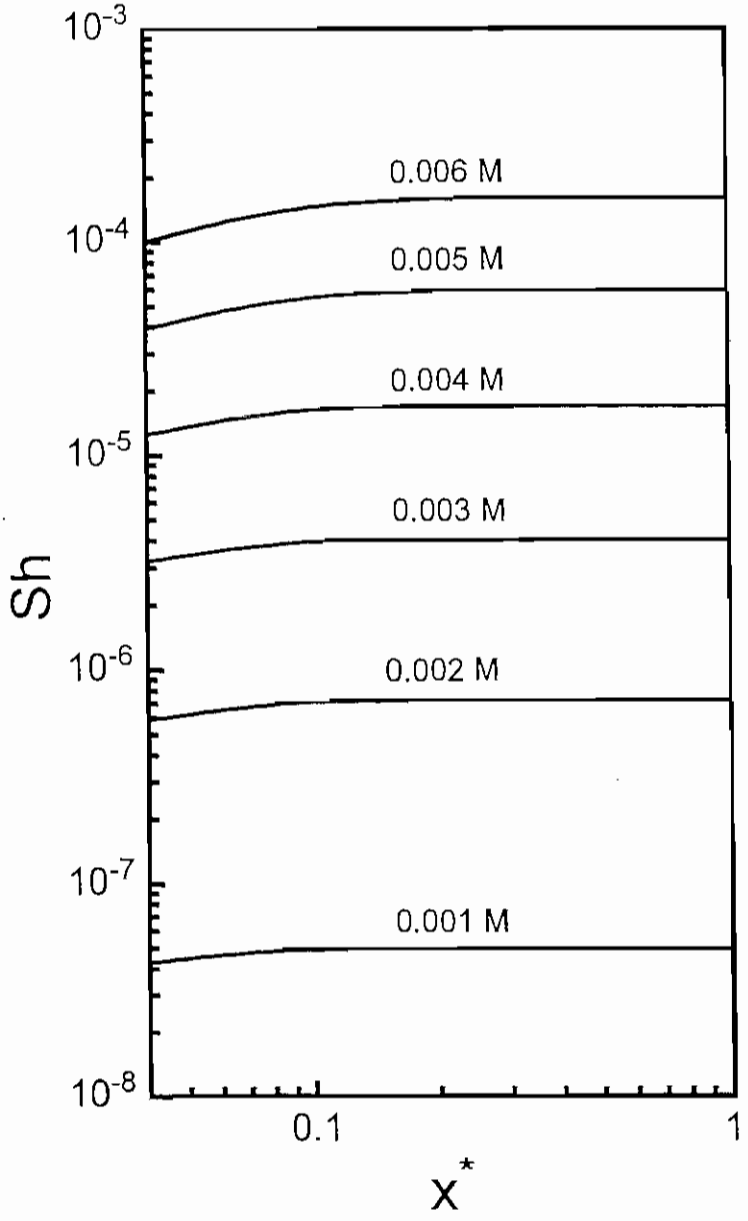
10-3
10-4
10-5
10-6
10-7
10-8
Sh
0.006 M
0.005 M
0.004 M
0.003 M
0.002 M
0.001 M
0.1
1
X*

Figure 5

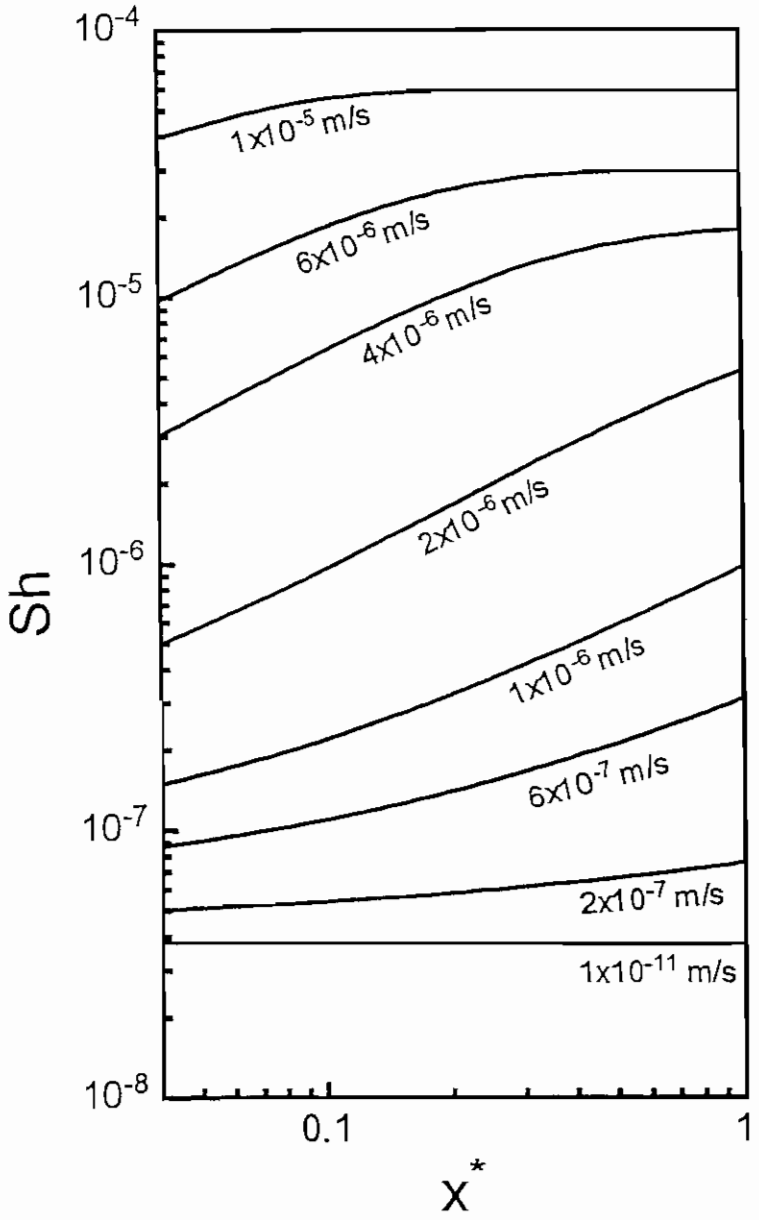
10^{-4}
10^{-5}
10^{-6}
10^{-7}
10^{-8}
Sh
1x10^{-5} m/s
6x10^{-6} m/s
4x10^{-6} m/s
2x10^{-6} m/s
1x10^{-6} m/s
6x10^{-7} m/s
2x10^{-7} m/s
1x10^{-11} m/s
0.1
1
x*

Figure 7

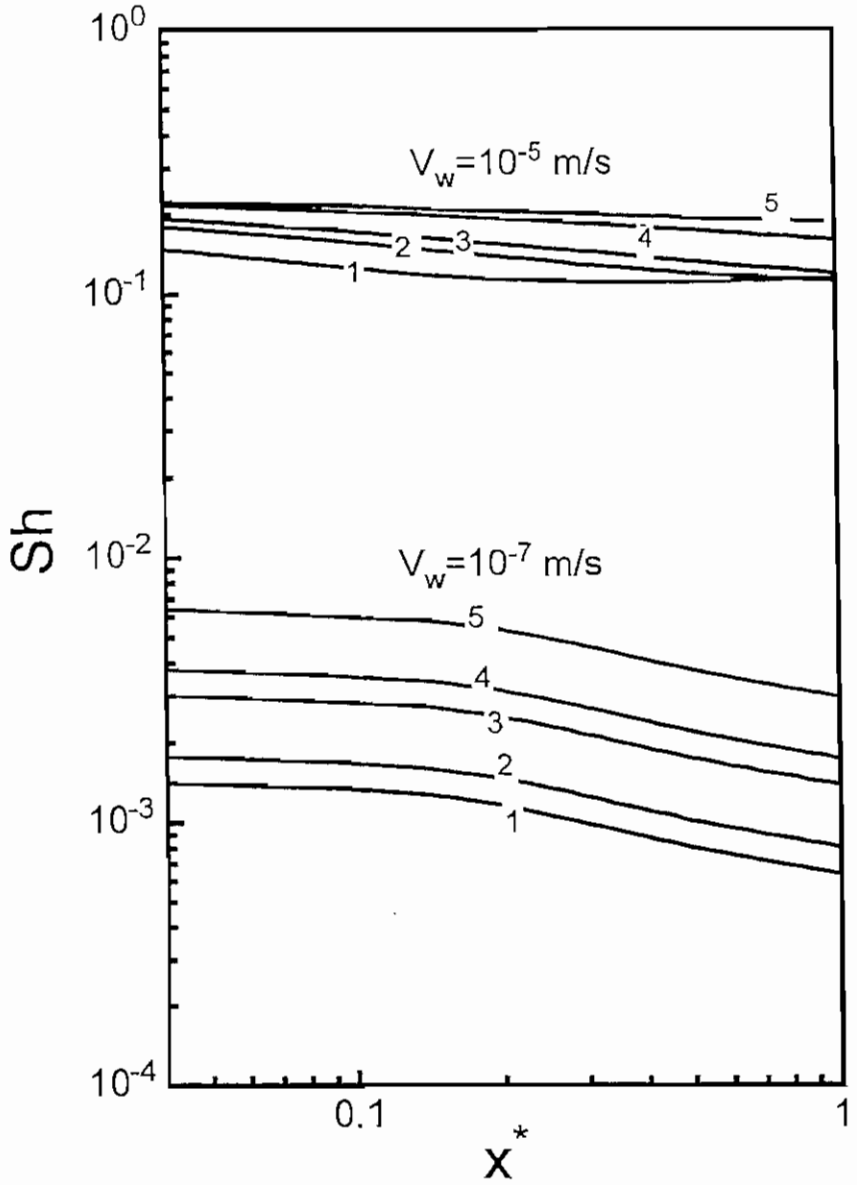

Figure 9

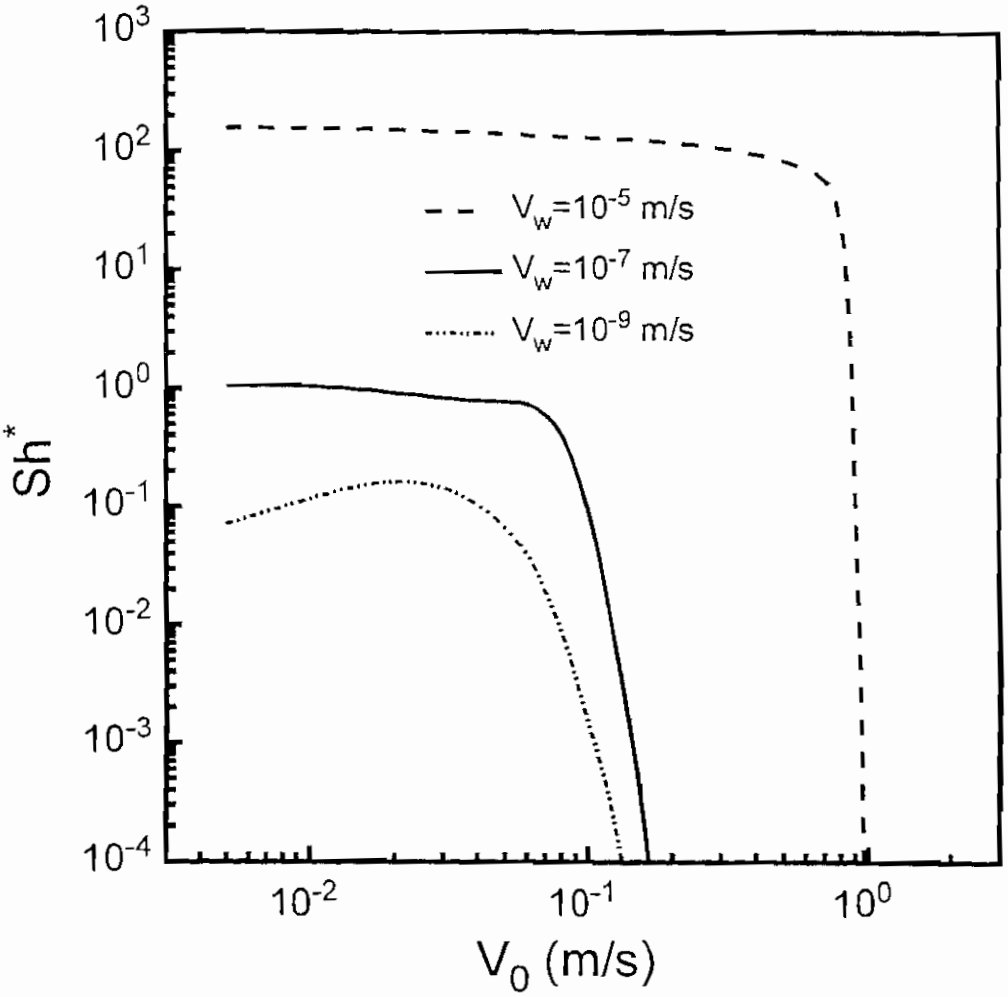
10^3
10^2
10^1
10^0
10^{-1}
10^{-2}
10^{-3}
10^{-4}
Sh*
$V_w=10^{-5}$ m/s
$V_w=10^{-7}$ m/s
$V_w=10^{-9}$ m/s
10^{-2}
10^{-1}
10^0
V_0 (m/s)

Figure 11

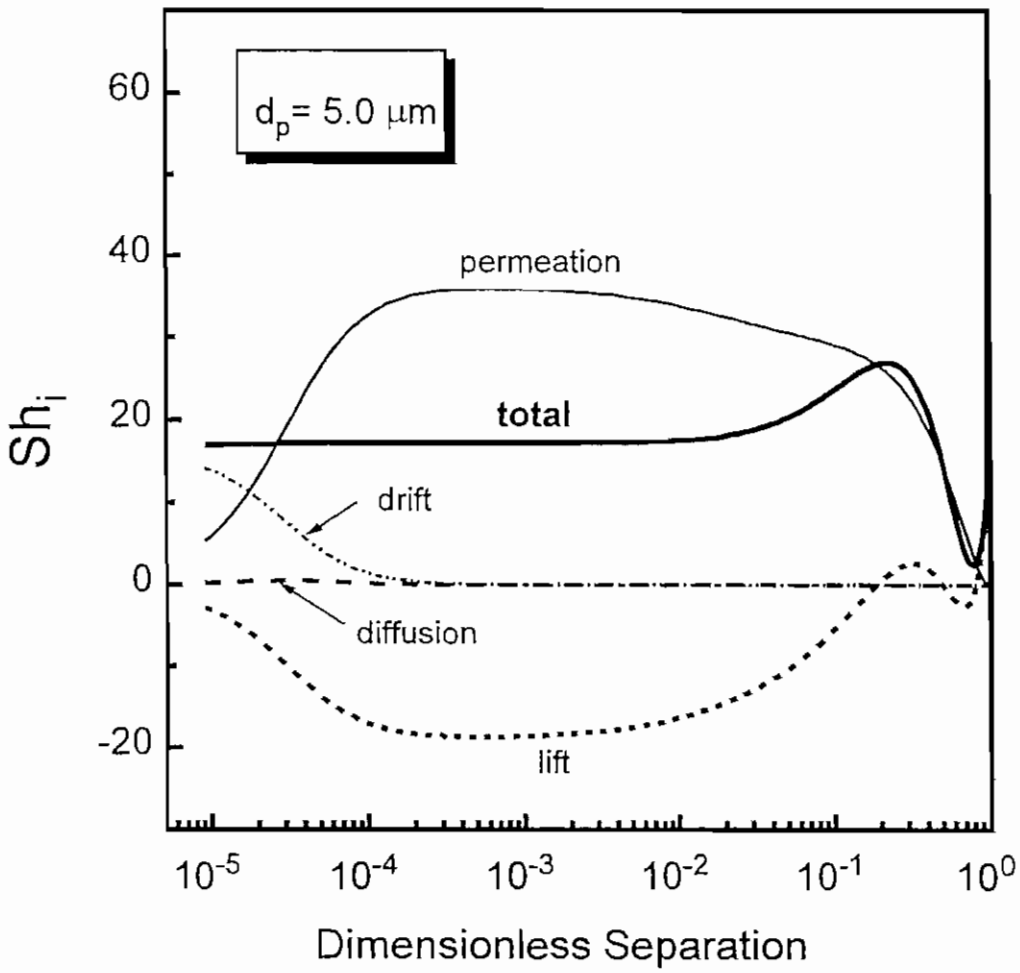
d_p= 5.0 μm
permeation
total
drift
diffusion
lift
60
40
20
0
-20
Sh_i
10^{-5}
10^{-4}
10^{-3}
10^{-2}
10^{-1}
10^{0}
Dimensionless Separation

Figure 13

Appendix IV

Elimelech, M., and Zhu, X., "Colloidal Fouling of Reverse Osmosis Membranes", presented at the ***Proceedings of the ASCE-1994 National Conference on Environmental Engineering***, July 11-13, 1994, pages 329-335.

Reprinted from CRITICAL ISSUES IN WATER AND WASTEWATER TREATMENT
Proceedings, 1994 National Conference on Environmental Engineering
Sponsored by the Environmental Engineering Div./ASCE
Held July 11-13, 1994, Boulder, Colorado

Colloidal Fouling of Reverse Osmosis Membranes

Menachem Elimelech and Xiaohua Zhu[1]

Abstract

Experiments on the fouling of thin film composite and cellulose acetate reverse osmosis membranes by aluminum oxide colloids are reported. Fouling was significant at high ionic strengths, resulting in reduced water flux and salt rejection. Under the chemical conditions tested, colloidal fouling was found to be reversible, thus providing an indirect evidence that pore blockage is not an important mechanism in colloidal fouling of reverse osmosis membranes. A qualitative model for colloidal fouling of reverse osmosis membranes is proposed.

Introduction

Polymeric reverse osmosis membranes are used extensively in numerous separation processes, including wastewater reclamation and seawater and brackish water desalination. Fouling is a major problem in reverse osmosis operation, resulting in product water flux decline and larger operating costs. Colloidal particles are considered to be the principal cause of membrane fouling. Fouling of reverse osmosis membranes places a large economic restriction on membrane plant operation. A key to this problem lies in a fundamental understanding of the physicochemical mechanisms of colloidal fouling.

[1] Department of Civil & Environmental Engineering, University of California, Los Angels, CA 90024-1593

The mechanisms of colloidal fouling are complex and poorly understood. The general objective of the study presented here is to identify the chemical-colloidal factors which control the rate of colloidal fouling of reverse osmosis membranes. More specifically, we will report on: (1) colloidal fouling experiments with model colloidal suspensions and solution chemistries using a laboratory reverse osmosis test unit; (2) identification of chemical-colloidal factors controlling colloidal fouling, and (3) postulating a qualitative model for colloidal fouling.

Experimental

Fouling tests were conducted with cellulose acetate and thin film composite membranes (supplied by *Hydranautics* and *Desalination Systems*). In these fouling experiments, aluminum oxide colloids at concentrations of 10, 30, and 100 mg/L were used. Experiments were conducted with three electrolyte concentrations: 0.001, 0.01, and 0.1 M NaCl (correspond to 58.5, 585, and 5845 ppm NaCl, respectively). In addition, some fouling experiments were conducted in the presence of humic substances. The net driving pressure (*i.e.*, the applied pressure minus the osmotic pressure) was maintained at 400 psi, so that the role of solution chemistry on the extent of colloidal fouling can be investigated without considering pressure effects.

In a typical reverse osmosis fouling test, a particle-free solution with the desired NaCl concentration was circulated through the membrane test unit at the desired flow and pressure. The fluid velocity over the membrane under the hydraulic conditions employed in the tests was 6.7 cm/s, resulting in a Reynolds number close to 590. After about 14 hours of operation at this mode, a concentrated stock suspension of particles was added to the feeding tank to establish a desired particle concentration. This was considered as the initial time of the fouling experiment. The flux just before adding the particles was the reference flux, and all other measured fluxes were referred to this one (*i.e.*, the relative flux is the actual flux at any time divided by this reference flux). Samples to determine the permeate flux and salt rejection were taken at various time intervals. In addition, samples from the feeding tank were taken once or twice a day to measure the particle size of the suspensions by dynamic light scattering.

Results and Discussion

Results of representative fouling tests are presented in Figures 1-3. In this figures, the relative water flux and salt rejection are presented as a function of time. These relative values are obtained by dividing the value of the flux or salt rejection at any time by the corresponding initial value (*i.e.*, just before adding the colloids to the suspension). After 100 hours, the membrane was rinsed with distilled water and the fouling test was resumed. The purpose of this step was to test the reversibility of colloidal fouling. Reversibility of colloidal fouling has direct implications for cleaning of colloid-fouled reverse osmosis membranes.

Figures 1 and 2 are for fouling of composite and cellulose acetate membranes at 0.1 M NaCl. It is demonstrated that after rinsing the membrane with deionized water the flux is restored. Our experiments showed that the thin film composite membranes display a moderate flux decline even in the absence of colloids, which explains why the water flux is not restored to the initial value after rinsing. Similar effects are observed in the fouling experiment with 0.1 NaCl and humic acid (0.6 mg/L TOC), as shown in Figure 3. It should be noted that in the presence of humic acid, the particles and membrane are negatively charged, while in the absence of humic acid the membrane is negatively charged while the particles are positively charged. From the results shown in Figures 1-3, it seems that the fouling behavior is controlled by the high ionic strength, regardless of the electrokinetic properties of the particles and membranes. It is further shown that the presence of a colloidal deposit layer on the membrane surface influences the salt passage through the membrane. A slight decrease in salt rejection is observed. The decrease in salt rejection is attributed to the enhanced concentration polarization caused by the presence of retained particles.

Additional fouling experiments at low and moderate ionic strengths were conducted. The fouling behavior observed in our experiments was related to the solution chemistry and the electrokinetic charge of particles and membranes. Four possible combinations of particle and membrane charges and ionic strengths can be described when particles interact with reverse osmosis membranes. These combinations and their presumed impact on fouling are discussed below.

Low ionic strength; particles and membranes are oppositely charged. In this case, particles deposit favorably onto the membrane surface. However, since the particles are stable at low ionic strengths, suspended particles

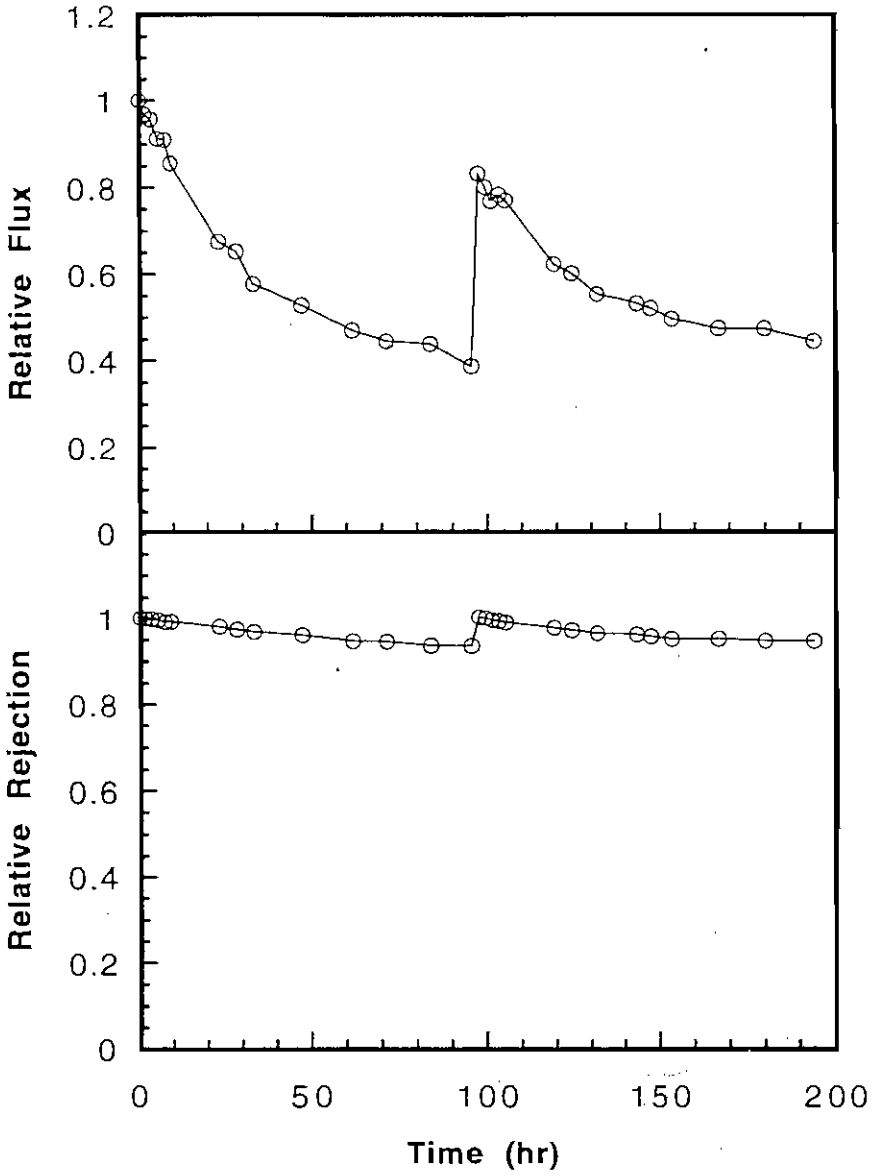

Figure 1. Relative flux and salt rejection of a fouling test with a thin film composite reverse osmosis membrane. Experiment was conducted with a 10 mg/L aluminum oxide colloidal suspension and 0.1 M NaCl solution.

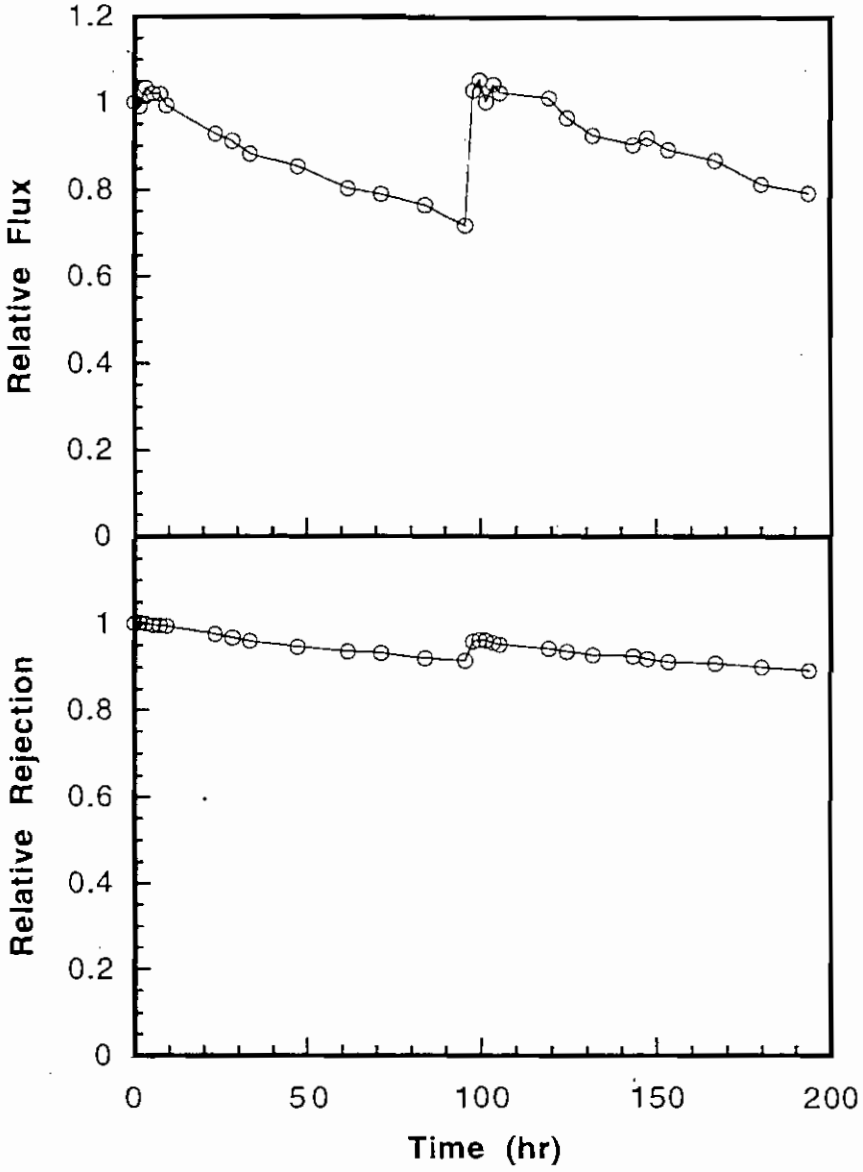

Figure 2. Relative flux and salt rejection of a fouling test with a cellulose acetate reverse osmosis membrane. Experiment was conducted with a 10 mg/L aluminum oxide colloidal suspension and 0.1 M NaCl solution.

cannot deposit onto retained particles. Particle deposition studies show that, for this "monolayer deposition", only a small fraction of the surface is covered by particles (Song and Elimelech, 1993). It is hypothesized that in this case there will be no significant water flux decline. Some increase in the salt passage may occur due to the presence of particles on the membrane.

Moderate to high ionic strength; particles and membranes are oppositely charged. As in the previous case, the deposition of particles onto the membrane surface is favorable. Furthermore, since the particles are unstable at high ionic strength, the deposition of particles onto previously retained particles is also favorable. This deposition behavior will probably result in a thick fouling layer, the thickness of which is highly dependent on the hydrodynamic conditions. It is hypothesized that, in this case, there will be a significant water flux decline and an increase in salt passage.

Low ionic strength; particles and membranes are similarly charged. In this case, particle deposition onto the membrane is significantly hindered by repulsive double layer interactions. There will be no buildup of a fouling layer on the membrane surface and it is presumed that no water flux decline will be observed.

High ionic strength; particles and membranes are similarly charged. At high ionic strengths, the repulsive double layer interactions between particles and the membrane surface and between suspended and retained particles are low. As a result, particles can accumulate on the membrane surface and form a thick fouling layer. It is hypothesized that, in this case, there will be a significant water flux decline and an increase in salt passage.

Acknowledgment

The research reported here was funded by the State of California, Department of Water Resources; the National Water Research Institute; and the University of California, Water Resources Center.

References

Song, L., and Elimelech, M. (1993). "Dynamics of Colloid Deposition in Porous Media: Modeling the Role of Retained Particles", *Colloids Surfaces A: Physicochem. Eng. Aspects,* **73**, 49-63.